

ISSN: 2164-5388

Volume 10, Number 2, April 2020



Open Journal of Biophysics

BIOPHYSICS

ISSN: 2164-5388



9 772164 1538002 02

<https://www.scirp.org/journal/ojbiphy>

Journal Editorial Board

ISSN Print: 2164-5388 ISSN Online: 2164-5396

<https://www.scirp.org/journal/ojbiph>

Associate Editors

Dr. Veysel Kayser	Massachusetts Institute of Technology, USA
Prof. Ganhui Lan	George Washington University, USA
Dr. Jaan Männik	University of Tennessee, USA
Prof. Sanbo Qin	Florida State University, USA
Dr. Bo Sun	Oregon State University, USA
Dr. Bin Tang	South University of Science and Technology of China, China

Editorial Board

Prof. Rabiul Ahasan	University of Oulu, Finland
Prof. Abass Alavi	University of Pennsylvania, USA
Prof. Chris Bystroff	Rensselaer Polytechnic Institute, USA
Dr. Luigi Maxmilian Caligiuri	University of Calabria, Italy
Prof. Robert H. Chow	University of Southern California, USA
Prof. Carmen Domene	University of Oxford, UK
Prof. Antonio José da Costa Filho	University of São Paulo, Brazil
Dr. John Kolega	State University of New York, USA
Prof. Pavel Kraikivski	Virginia Polytechnic Institute and State University, USA
Dr. Gee A. Lau	University of Illinois at Urbana-Champaign, USA
Prof. Yves Mély	Louis Pasteur University, France
Dr. Monalisa Mukherjea	University of Pennsylvania, USA
Dr. Xiaodong Pang	Florida State University, USA
Prof. Arthur D. Rosen	Indiana University, USA
Prof. Brian Matthew Salzberg	University of Pennsylvania, USA
Prof. Jianwei Shuai	Xiamen University, China
Prof. Mateus Webba da Silva	University of Ulster, UK
Prof. Alexander A. Spector	Johns Hopkins University, USA
Prof. Munekazu Yamakuchi	University of Rochester, USA

Table of Contents

Volume 10 Number 2

April 2020

Exposure of Weak Time-Invariant Electromagnetic Fields to B16-BL6 Cell Cultures Alter Biophoton Emission Profile as a Function of Distance	
B. C. S. Yearington, V. L. Hossack, B. T. Dotta.....	47
Solar Radiation, Perelman Entropy Mapping, DNA, Viruses etc.	
K. W. Wong, P. C. W. Fung, W. K. Chow.....	54
The Quantum-Mechanical Sensitive Na/K Pump Is a Key Mechanism for the Metabolic Control of Neuronal Membrane Function	
S. Ayrapetyan.....	59
A Short Note on Containment Scheme against Spreading of Novel Coronavirus COVID-19	
W. K. Chow, C. L. Chow.....	84
COVID-19: A Physical Model	
K. W. Wong, P. C. W. Fung, W. K. Chow.....	88
DNA Sequencing Modified Method through Effective Regulation of Its Translocation Speed in Aqueous Solution	
L. Gasparyan, I. Mazo, F. Gasparyan, V. Simonyan.....	96

Open Journal of Biophysics (OJBIPHY)

Journal Information

SUBSCRIPTIONS

The *Open Journal of Biophysics* (Online at Scientific Research Publishing, <https://www.scirp.org/>) is published quarterly by Scientific Research Publishing, Inc., USA.

Subscription rates:

Print: \$79 per issue.

To subscribe, please contact Journals Subscriptions Department, E-mail: sub@scirp.org

SERVICES

Advertisements

Advertisement Sales Department, E-mail: service@scirp.org

Reprints (minimum quantity 100 copies)

Reprints Co-ordinator, Scientific Research Publishing, Inc., USA.

E-mail: sub@scirp.org

COPYRIGHT

Copyright and reuse rights for the front matter of the journal:

Copyright © 2020 by Scientific Research Publishing Inc.

This work is licensed under the Creative Commons Attribution International License (CC BY).

<http://creativecommons.org/licenses/by/4.0/>

Copyright for individual papers of the journal:

Copyright © 2020 by author(s) and Scientific Research Publishing Inc.

Reuse rights for individual papers:

Note: At SCIRP authors can choose between CC BY and CC BY-NC. Please consult each paper for its reuse rights.

Disclaimer of liability

Statements and opinions expressed in the articles and communications are those of the individual contributors and not the statements and opinion of Scientific Research Publishing, Inc. We assume no responsibility or liability for any damage or injury to persons or property arising out of the use of any materials, instructions, methods or ideas contained herein. We expressly disclaim any implied warranties of merchantability or fitness for a particular purpose. If expert assistance is required, the services of a competent professional person should be sought.

PRODUCTION INFORMATION

For manuscripts that have been accepted for publication, please contact:

E-mail: ojbiphy@scirp.org

Exposure of Weak Time-Invariant Electromagnetic Fields to B16-BL6 Cell Cultures Alter Biophoton Emission Profile as a Function of Distance

Billy C. S. Yearington, Victoria L. Hossack, Blake T. Dotta*

Behavioural Neuroscience and Biology Programs, Laurentian University, Sudbury, Canada

Email: *bx_dotta@laurentian.ca

How to cite this paper: Yearington, B.C.S., Hossack, V.L. and Dotta, B.T. (2020) Exposure of Weak Time-Invariant Electromagnetic Fields to B16-BL6 Cell Cultures Alter Biophoton Emission Profile as a Function of Distance. *Open Journal of Biophysics*, 10, 47-53.

<https://doi.org/10.4236/ojbiphy.2020.102004>

Received: January 18, 2020

Accepted: February 21, 2020

Published: February 24, 2020

Copyright © 2020 by author(s) and Scientific Research Publishing Inc.

This work is licensed under the Creative Commons Attribution International License (CC BY 4.0).

<http://creativecommons.org/licenses/by/4.0/>



Open Access

Abstract

Biophoton emission is produced by all living systems; this emission pattern has been shown to be altered by the presence of an electromagnetic field (EMF). Cultures of B16-BL6 cells were exposed to a weak EMF produced by a specially constructed EM generator, called the “Resonator”, for one hour. This EM generator incorporates multiple geometric ratios in its design, including the golden ratio (ϕ), π , root 2, root 3, and root 5. It has been used previously to purify water of toxins. There was a significant decrease in mean photon counts from B16-BL6 cells exposed at a distance of 1 m compared to those exposed at 0 m. Alterations in the spectral power density variability were also observed in the 8 - 10 Hz range. The EM generator may have an impact on the viability of the exposed cell cultures, but only at specific distances.

Keywords

Electromagnetic Fields, B16-BL6 Cells, Spectral Power Density, Biophoton Emission

1. Introduction

All living biological systems emit low levels of electromagnetic radiation, referred to as biophoton emission. It has been proposed that metabolic activity is the primary source of biophoton emission, specifically the oxidation of free radicals. This is supported by experimental evidence including the addition of hydrogen peroxides to tissue, or a reduction of tissue antioxidants [1]. This pro-

posed mechanism is the same for both types of biophoton emission: spontaneous and induced. Spontaneous biophoton emission is produced by the natural metabolic activity of the organism. Induced biophoton emission is observed after an organism has been exposed to one or more of several factors, which can be natural or artificial. These factors include bacterial or viral infection, stress, external temperature, and ionizing radiation, to name a few [2]. Electromagnetic fields (EMFs) have also been previously demonstrated to induce biophoton emission in combination with specific wavelengths of light [3].

The examination of the effect of exposure to an EMF alone on biophoton emission has not been done. In an experiment by Karbowski and colleagues, three complex, time-varying EMF patterns were used [3]. The central effect observed was the increase in mean photon counts when B16-BL6 cells were exposed to a combination of both an EMF and 450 nm light. In this experiment, the aim was to focus on the characteristics of a single EMF. Additionally, previous experiments by Persinger and colleagues [4] have demonstrated an inverse relationship between photon flux densities and nanotesla magnetic fields over cell aggregates. This experiment illustrated a conservation of energy effect between the measured geomagnetic field and the added—or subtracted—changes in photon emission intensity from nearby cells.

The EMF used in this experiment, was generated by a novel device invented by Dr. K. Shallcross. This EM generator, referred to as the “Resonator”, uses a series of metallic roller magnets arranged at specific angles to create a pattern derived from a sacred geometry. Sacred geometry refers to numerical values derived from simple geometric relations, such as π , $\sqrt{2}$, $\sqrt{5}$, and [5]. When the device is on, the roller assemblies rotate, which generates a weak EMF, in the range of 1 μ T to 10 μ T. When the device is off, no EMF is generated.

Previous experiments with the “Resonator” have shown differential effects on the growth rate of bacterial cultures [6]. Three of the examined bacteria species were shown to have an increased growth rate after exposure, while one species had a decreased growth rate. This suggests that the complexity of the “Resonator” field is such that it can have opposite effects on different species. This is most likely mediated via different effects on cellular metabolic pathways.

In addition, exposure of the “Resonator” EMF to B16-BL6 cells for three hours has been shown to significantly decrease cell viability [7]. Takeda and colleagues have demonstrated that biophoton emission in cancerous cells was related to the population size [8]. Thus, if exposure to the “Resonator” EMF is correlated with decreased cell viability, and biophoton emission is correlated with cell population, there should be an observable decrease in the biophoton emission of exposed cell cultures.

2. Methods

B16-BL6 cell cultures were grown in DMEM supplemented with 10% fetal bovine serum and 1% antibiotics on 10 mm Petri dishes and allowed to reach con-

fluence in a water-jacket copper-lined incubator at 37°C (95% air, 5% CO₂). Cell cultures were grown on Petri dishes in groups of 16. Once confluent, the plates were removed from the incubator and placed into one of four conditions: Field 1 m, Field 0 m, Sham 1 m, Sham 0 m. Each condition contained four cell plates. These conditions refer to the state of the “Resonator”, either with an active magnetic field in the Field conditions, or with the device turned on but with no movement of the coils; these were the Sham conditions. The cell plates were placed on a table at either 1m or 0 m from the “Resonator”. Vertically, the cell plates were separated from the “Resonator” by a distance of approximately 10 - 15 cm. The distance of vertical separation was constant between the 1m and 0m conditions. The plates were arranged side by side, such that they formed an approximate square on the surface of the table. This table did not make physical contact with the “Resonator” to remove any vibrational effects from the spinning of the “Resonator” coils. The “Resonator” was then turned on for the Field conditions. Cell plates were left on the table for no less than one hour.

Once the exposure was complete, the biophoton output of the cell plates was immediately measured. This measurement was performed in the experimental chamber, a specially constructed space measuring 1.32 m long, 1.27 m wide, and 1.70 m in height. Before the experimental chamber was opened, a baseline measurement was taken. The cell plate was placed on a small polystyrene box, which is located on a chair in the centre of the experimental chamber. The sample was measured with four PMTs, which were located on three walls and the ceiling of the experimental chamber. Each PMT was separated from the sample by a distance of 15 cm. A one-minute delay between the closure of the experimental chamber and the start of the measurement ensured minimal light contamination of the cell plate measurement. Each cell plate was measured for two minutes. Including the one-minute delay, each plate was in the experimental chamber for three minutes. After each plate had been measured, a post baseline measurement was performed. This procedure was identical to the cell plate measurement, including the one-minute delay. Field and sham measurements for plates exposed at any given distance were recorded on the same day to minimize daily variations.

Data from the measurement sessions was exported into IBM SPSS for statistical and spectral analyses.

3. Results

All of the analyses below were performed with the data from the PMT located at the Head position. Only the second minute of the measurement was used for analyses. A total of 14 cases from two different days were removed due to outlier effects. This gave a total N of 41.

First, a comparison was made between the baseline condition and all cell conditions. A Student's t test for independent samples revealed a significant difference between the baseline and the cell conditions ($t = -6.260$, $p < 0.001$, $\eta^2 =$

0.445). The cell condition had significantly higher mean photon counts than the baseline condition. This is shown in **Figure 1**.

To expand on the B16-BL6 conditions, a pair of Student's *t* tests for independent samples were used to compare mean photon counts between field condition and distance. This is shown in **Figure 2**. There was no significant difference in mean photon counts between the Sham 0m condition and the Sham 1 m condition ($t_{(14)} = 0.163$, $p = 0.873$). The mean photon counts of the Field 1 m condition were significantly lower than the Field 0 m condition ($t_{(18)} = 2.120$, $p = 0.048$, $r^2 = 0.200$).

A series of one-way ANOVAs were performed to compare the spectral power density variability by condition membership. The spectral power density variability is the standard deviation of the spectral power density, per case. For this procedure, the spectral power density variability was averaged into multiple

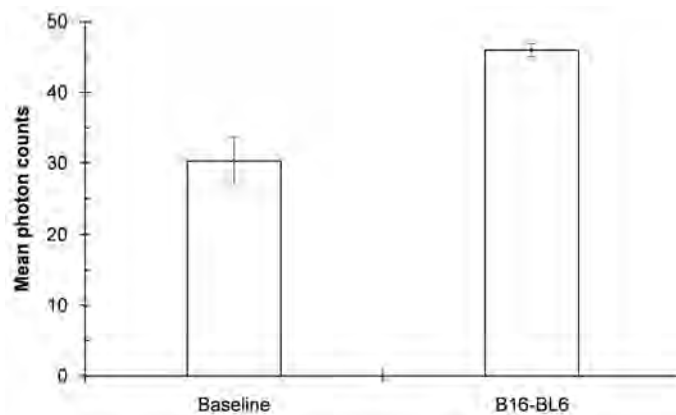


Figure 1. Comparison of the mean photon counts between the baseline condition and all B16-BL6 conditions. The B16-BL6 condition was significantly higher than the baseline condition. Error bars represent standard error of the mean; $n = 5$ for baseline, $n = 36$ for B16-BL6.

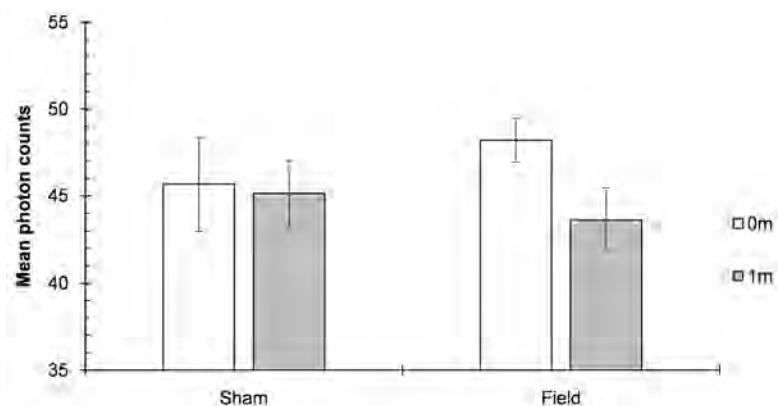


Figure 2. Comparison of the mean photon counts between Sham and Field conditions at 0 m and 1 m. There was no significant difference between the Sham 0 m and Sham 1 m conditions; the Field 1 m condition was significantly lower than the Field 0 m condition. Error bars represent standard error of the mean; the n for each condition was 8, 8, 12, and 8, respectively.

frequency bins, each with a width of 1 - 4 Hz. The only bin that produced a significant main effect was the low alpha (8 - 10 Hz) frequency bin ($F_{(3,32)} = 4.047$, $p = 0.015$, $\eta^2 = 0.255$). Post-hoc tests revealed the effect was being driven by the difference between the Sham 1m and Field 1 m conditions ($p < 0.05$). This is shown in **Figure 3**.

4. Discussion

The mean photon counts from B16-BL6 cell cultures were significantly higher than the baseline, regardless of experimental conditions. It is evident that the presence of a biological system increases the mean photon count as measured by the PMT. This is consistent with previous findings.

A comparison of mean photon counts between the experimental conditions revealed novel results. The sham conditions were not significantly different from one another, which would be expected. The proximity to the static EMF produced by the “Resonator”, while inactive, did not seem to impact the mean photon counts.

The field conditions exhibit distance effects. The Field 1 m condition had significantly lower mean photon counts compared to the Field 0 m condition. There are three possible interpretations: one, the induced EMF from the “Resonator” at 0 m led to increased mean photon counts in the Field 0 m condition; two, the induced EMF from the “Resonator” at 1 m led to decreased mean photon counts in the Field 1 m condition; three, a combination of effects one and two. Another factor to be considered is the impact of vibrational effects. Vibrational effects have been implicated in a possible mechanism of “Resonator”-cell interaction [7]. Thus, vibrational effects may interpose themselves with the EMF

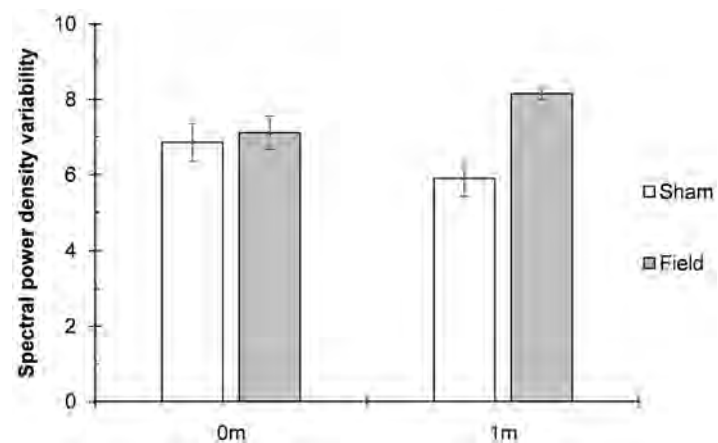


Figure 3. Comparison of the spectral power density variability in the low alpha frequency bin. There was a significant difference between the four conditions; post-hoc tests revealed the significance was being driven by the Sham 1 m and Field 1 m conditions. The Field 1 m condition spectral power density variability was significantly higher than the Sham 1 m condition. Both Sham and Field 0 m conditions were not significantly different from any other conditions. Error bars represent standard error of the mean; the n for each condition was 8, 8, 12, and 8, respectively.

effects while the “Resonator” is active; however, the plates were not placed in direct contact with the “Resonator” to minimize the effects of vibration.

The spectral power density of the four conditions was compared with a series of one-way ANOVAs; no significant differences were found. The variability of the spectral power density was also compared in a similar fashion; a significant effect was found in the low alpha frequency bin. This frequency bin was an average of the spectral power density variability scores in the 8 - 10 Hz frequency range. Post-hoc Tukey HSD revealed that the effect was driven by the Sham 1 m and Field 1 m conditions. The spectral power density variability was significantly higher in the Field 1 m condition compared to the Sham 1 m condition.

The implications of these two effects, mean photon counts and spectral power density variability, are centred on the Field 1 m condition. This condition had significantly lower mean photon counts than the Field 0 m condition, and significantly higher spectral power density variability than the Sham 1 m condition. This implies fewer photons are being released and the rhythmicity of photon emission in the 8 - 10 Hz range is less consistent. If the B16-BL6 cells’ metabolic activity is altered by the generated EMF, this may explain why the counts were lowered in the Field 1 m condition. The EMF that is generated is an extremely low-frequency field which does not change as a function of position (relative to the “Resonator”), although the intensity decreases with distance. This is a significant quality, since the signal pattern and frequency remain consistent over distance, the only EMF factor that would change between the Field 0 m and Field 1 m conditions is the intensity of the field.

It is important to mention that the spectral power density variability of the Sham conditions was not significantly different from the spectral power density variability of the Field conditions. This may be a function of low sample size. High variability is also a common issue when biophoton emission is involved. This is often why spectral analyses are performed. The cell cultures were removed from the incubator for exposure and for measurement. Ideally, both of these processes should be carried out in a temperature-controlled environment.

This experiment was meant to act as a brief observation of the biophoton emission patterns produced by the B16-BL6 cell cultures. As such, no cellular observations were made. Future experiments should include cell counts and viability. Comparisons could then be made directly between cellular variables and measured photon activity.

Conflicts of Interest

The authors declare no conflicts of interest regarding the publication of this paper.

References

- [1] Alipour, A. (2015) Demystifying the Biophoton-Induced Cellular Growth: A Simple Model. *Journal of Advanced Medical Sciences and Applied Technologies*, **1**, 112-115. <https://doi.org/10.18869/nrip.jamsat.1.2.112>

-
- [2] Cifra, M. and Pospisil, P. (2014) Ultra-Weak Photon Emission from Biological Samples: Definition, Mechanisms, Properties, Detection and Applications. *Journal of Photochemistry and Photobiology B: Biology*, **139**, 2-10. <https://doi.org/10.1016/j.jphotobiol.2014.02.009>
- [3] Karbowski, L.M., Murugan, N.J. and Persinger, M.A. (2016) Experimental Evidence That Specific Photon Energies Are Stored in Malignant Cells for an Hour: The Synergism of Weak Magnetic Field-LED Wavelength Pulses. *Biology and Medicine*, **8**, BM-162-16.
- [4] Persinger, M.A., Dotta, B.T., Karbowski, L.M. and Murugan, N.J. (2015) Inverse Relationship between Photon Flux Densities and nanoTesla Magnetic Fields Over Cell Aggregates: Quantitative Evidence for Energetic Conservation. *FEBS Open Bio*, **5**, 413-418. <https://doi.org/10.1016/j.fob.2015.04.015>
- [5] Shallcross, K. (2016) Canadian Patent No. CA 2631215. Canadian Intellectual Property Office, Ottawa, ON.
- [6] Tessaro, L.W.E., Murugan, N., Persinger, M.A. (2015) Bacterial Growth Rates Are Influenced by Cellular Characteristics of Individual Species When Immersed in Electromagnetic Fields. *Microbiological Research*, **172**, 26-33. <https://doi.org/10.1016/j.micres.2014.12.008>
- [7] Tessaro, L.W.E., Karbowski, L.M., Lafrenie, R.M. and Persinger, M.A. (2015) Application of Dynamic Magnetic Fields to B16-BL6 Melanoma Cells Linked with Decrease in Cellular Viability after short Exposures. *Journal of the International Association of Advanced Technology and Science*, **1**, 1-11.
- [8] Takeda, M., Tanno, Y., Kobayashi, M., Usa, M., Ohuchi, N., Satomi, S. and Inaba, H. (1998) A Novel Method of Assessing Carcinoma Cell Proliferation by Biophoton Emission. *Cancer Letters*, **127**, 155-160. [https://doi.org/10.1016/S0304-3835\(98\)00064-0](https://doi.org/10.1016/S0304-3835(98)00064-0)

Solar Radiation, Perelman Entropy Mapping, DNA, Viruses etc.

Kai W. Wong¹, Peter C. W. Fung², Wan K. Chow³

¹Department of Physics and Astronomy, University of Kansas, Lawrence, USA

²Department of Physics, Department of Medicine, and Centre on Behavioral Health, University of Hong Kong, Hong Kong, China

³Department of Building Services Engineering, The Hong Kong Polytechnic University, Hong Kong, China

Email: kww88ng@gmail.com

How to cite this paper: Wong, K.W., Fung, P.C.W. and Chow, W.K. (2020) Solar Radiation, Perelman Entropy Mapping, DNA, Viruses etc. *Open Journal of Biophysics*, 10, 54-58.

<https://doi.org/10.4236/ojbiphy.2020.102005>

Received: February 10, 2020

Accepted: March 13, 2020

Published: March 16, 2020

Copyright © 2020 by author(s) and Scientific Research Publishing Inc.

This work is licensed under the Creative Commons Attribution International License (CC BY 4.0).

<http://creativecommons.org/licenses/by/4.0/>



Open Access

Abstract

A short note based on the homogeneous 5D space-time topological mappings is extended to cover DNAs of viruses and how the body's immune system can be enhanced to recognize and remove it.

Keywords

5D Homogeneous Space-Time and Perelman Mappings, Nitrogenous Bases, DNA, Viruses, Coronavirus, Immune System

Recently for the first time a detailed picture of the solar surface was observed via frequency patent analysis. It was found that its intensity patent resembles that of the Sunflower (see **Figure 1**).

While it is not expected, it actually represents the geometric patent of the result from Perelman Quantum entropy mapping that gives us the Poincare sphere, via the breaking of the Maxwell monopole potential fields. We refer our readers to the published articles [1] [2] [3] [4]. The results can be summarized from the breaking of the 5D quantum homogeneous space-time manifold vector field potentials as given by the direct product of the 4 Maxwell E-M potentials with the Maxwell monopole potentials into the non-homogeneous $\{SU(2) + SU(3)\} \times L$ obtained via the dimension reduction projections P_0 and P_1 as discussed in [3] [4]. It is through such projections and the conserving of gauge invariance as required by the coupling between the vector and e-trino [1] spinor solutions that matter as represented by hadrons and leptons are produced. And through the requirement of maintaining charge neutrality as given by the 5D homogeneous space-time, elements and complex molecules are formed in place of a homogeneous matter distribution. In fact the lowest two Poincare quantum

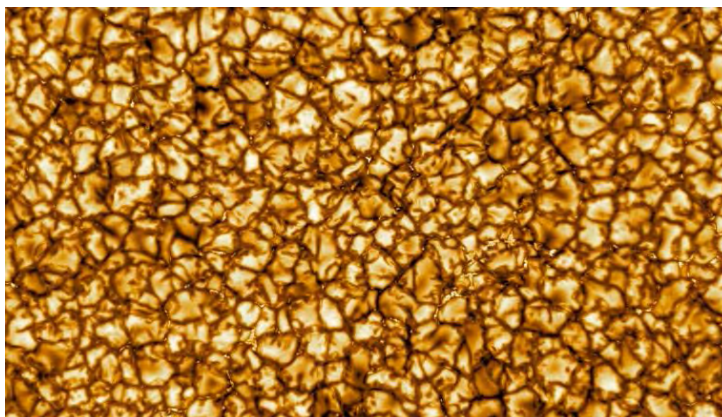


Figure 1. Solar surface (image source: <https://www.nationalgeographic.com/science/2020/02/sun-still-burning-mystery-may-be-about-to-change-solar-orbiter-launch/>).

spheres formed through Perelman mappings [2] and through the application of Gell-Mann standard model [5] are that of the Carbon 12 nucleus as geometrically represented by the hard sphere dense packing [6], while the next level is that given by the Bucky Ball surface of protons and neutrons. It is then easy to see that the fundamental patterns on the Poincare spherical surface are simply that of the hexagon and the pentagon (see **Figure 2** and **Figure 3**).

The basic matter creation then splits the energy domain of the monopole fields, resulting in leaving the energy portion that is less than the rest mass of the electron still could be preserving the homogeneous 5D symmetry. It is only through the further spherical space geometrical symmetry breaking into $2D \times 1D$, and the maintenance of gauge invariance that we are led to the formation of the four basic nitrogenous bases [7], essential to the creation of DNAs obtained from the random stacking of the bases and thereby creates the life forms. In order to achieve that 2D space symmetry for the nitrogenous bases, we establish the normal by adding two neutrons on opposite equilateral triangles in C12 shell, creating C14; thus all life forms contain C14. While for the Buckyball shell, neutrons can be added to centers of the pentagons, making a sphere with spikes. In the bio micro-scale, these spikes contain the RNAs. The identification of each life form is then given by the frequency spectra, which in turn is completely determined by the quantum phase matching tunneling of the Diagonal-Long-Range-Order, DLRO, monopole fields strength, formed from two opposite charge and momenta massless spinous, that is the *etrino* and *anti-etrino*, with a total angular momentum 1, similar to the photon and therefore depends explicitly on the length of each section of random stacking of the nitrogenous bases and the matching quantum tunneling phases in its DNAs. The life form's genome number is thus given by $2 \times 7! \times 3 = 30240$, where the factor 3 comes from the photon angular momentum, and the factor 7 is because the end caps must be only given by the end nitrogenous base Thymine, with only a single transmission face. It is via the DLRO boson state that induces the

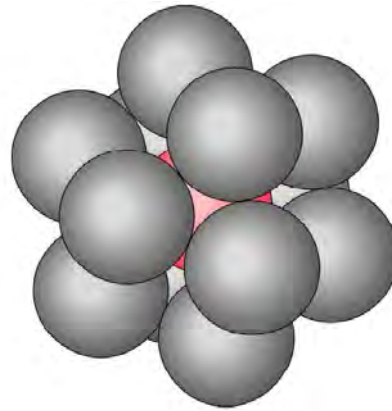


Figure 2. C12 hard sphere dense packing model (Wong *et al.* 2014, ref. [1]).



Figure 3. The 20 hexagons are in white, while the 12 isolated pentagons are in black.

Off-Diagonal-Long-Range-Order, ODLRO in the chemical valence band states provided by the electronic p waves in the carbon of the bio-matter that then leads to the natural growth of biological cells, body tissues, organs and structure [8] [9]. Thus each life possesses a unique set of cell structures identified by its DNAs spectrum. Any non-compliance should be detected by the body's natural immune systems and eliminated from self reproduction. But due to the infinite choices in the varying spectra possible, certain closed foreign DNAs are frequently missed by the immune system detection. It is this problem that leads to the invasion of foreign DNAs that can be separated into non-cell structure viruses, such as the common flus, SAR and the recent coronavirus, etc. provided the effective body's thermal temperature $T < T_c$ of the virus critical temperature for growth, thus allowing it to multiply within the body leading usually to destruction of the lung cells and the prevention of the body's respiratory natural oxidation process in the removal of the dead cells within the body. Meaning these viruses always disrupt the body's respiratory function, because from PV/T constrain as PV decrease, where P and V are air pressure and volume of the lung respectively, so will T , enhancing the virus reproduction. Thus the coronavirus might behave like the common flu and is perhaps seasonal. While other foreign DNAs left within the body coupled to the cell and tissue growth would result in

cancerous growth of the body. Because of these, there are numerous potential harms that can cause the death of life without making the immune system recognizing and remove these foreign DNAs. Understanding the fundamental physics could guide us to develop proper cure and preventions. Take as an example, small pox vaccine was derived from dead tissues formed from small pox. The current coronavirus, is supposed to be originated from the bat biting of the snake that created this virus and passes it onward to human. Normally in the wild, that could be a frequent occurrence. But the bitten snake dies and the virus with it disappeared. Yet in a market, both snakes and other animals are placed in contact, hence leading to the virus being spread and multiplied. If true, it means the COVID-19 can start anywhere, even without human transmission. This coronavirus is unique in that it composes the DNA spectra from the warm blooded bat to that of the cold blooded snake. Cold blooded animal is similar to plants, as such part of its DNA spectra must contain that is the visible portion of spectrum as provided by the solar photo spectrum. Meaning this coronavirus DNA is unlike the SAR and EBOLA, which have DNA spectra covering only those of warm blooded mammals, must contain such optical photon frequency portion also. Hence photo UV irradiation will not kill the coronavirus. The human body's immune system would be activated if it recognizes it as being foreign. Since human is warm-blooded, it is more likely for its immune system to detect this virus and respond to eliminate it, unless that human body immune system is weak. Perhaps this explains why the coronavirus so far indicated is far less deadly than SAR or EBOLA, and it does not seem to be deadly for the young as their immune system and lung are still developing? To see how we can normally strengthen our immune system to beat back the Coronavirus, we can fall back on what we know. If we consume raw honey which is sugar obtained by the bees pollination of different flowers, it could stimulate the body's immune system to recognize those plant's DNA that possesses spectrum in the visible and UV range, which might even cover that of the coronavirus? In fact by analyzing a virus DNA spectrum we can create medications by matching certain known immune enhancement medication or food that will induce the human body immune system to recognize and remove it.

Acknowledgements

We thank Ms. Winnie So for her great help in preparing the manuscript.

Conflicts of Interest

The authors declare no conflicts of interest regarding the publication of this paper.

References

- [1] Wong, K.W., Dreschhoff, G.A.M. and Jungner, H. (2014) The Five Dimension Space-Time Universe—A Creation and Grand Unified Field Theory Model. Scien-

tific Research Publishing, Wuhan.

- [2] Wong, K.W., Dreschhoff, G., Jungner, H., Fung, P.C.W. and Chow, W.K., (2018) The Magnetic Monopole in 5D Homogeneous Space-Time. *Physics Essays*, **31**, 493-495. <https://doi.org/10.4006/0836-1398-31.4.493>
- [3] Perelman, G. (2002) The Entropy Formula for the Ricci Flow and Its Geometric Application. arXiv.math.DG/0211159.
Perelman, G. (2003) Ricci Flow with Surgery on Three-Manifolds. arXiv.mathDG/0303109.
- [4] Wong, K.W., Fung, P.C.W. and Chow, W.K., (2019) A Quantum Representation of the Homogeneous 5D Manifold and the Perelman Mappings of 5D onto Non-Homogeneous Lorentz 4D Manifolds. *Journal of Modern Physics*, **10**, 557-575. <https://doi.org/10.4236/jmp.2019.105039>
- [5] Gell-Mann, M. (1964) Nonleptonic Weak Decays and the Eightfold Way. *Physical Review Letters*, **12**, 155-156. <https://doi.org/10.1103/PhysRevLett.12.155>
- [6] Wong, K.W. (1964) Application of Nonlocal Field Operators to a System of Hard Sphere Bose Gas. *Journal of Mathematical Physics*, **5**, 637-642. <https://doi.org/10.1063/1.1704157>
- [7] Wong, K.W., Fung, P.C.W. and Chow, W.K. (2019) 5D Model Theory for Creating of Life Forms. *Journal of Modern Physics*, **10**, 1548-1565. <https://doi.org/10.4236/jmp.2019.1013103>
- [8] Ching, W.Y., Xu, Y.N., Zhao, G.L., Wong, K.W. and Zandiehnam, F. (1987) Electronic Structure and Excitonic-Enhanced Superconducting Mechanism in $\text{YBa}_2\text{Cu}_3\text{O}_{7-\delta}$. *Physical Review Letters*, **59**, 1333-1336. <https://doi.org/10.1103/PhysRevLett.59.1333>
- [9] Wong, K.W. and Ching, C.W. (1989) The Theory of Simultaneous Excitonic-Superconductivity Condensation. *Physica C*, **158**, 1-14. [https://doi.org/10.1016/0921-4534\(89\)90294-3](https://doi.org/10.1016/0921-4534(89)90294-3)

The Quantum-Mechanical Sensitive Na/K Pump Is a Key Mechanism for the Metabolic Control of Neuronal Membrane Function

Sinerik Ayrapetyan

Life Sciences International Postgraduate Educational Center, UNESCO Chair in Life Sciences, Yerevan, Armenia

Email: info@biophys.am

How to cite this paper: Ayrapetyan, S. (2020) The Quantum-Mechanical Sensitive Na/K Pump Is a Key Mechanism for the Metabolic Control of Neuronal Membrane Function. *Open Journal of Biophysics*, 10, 59-83.

<https://doi.org/10.4236/ojbiphy.2020.102006>

Received: February 12, 2020

Accepted: March 17, 2020

Published: March 20, 2020

Copyright © 2020 by author(s) and Scientific Research Publishing Inc. This work is licensed under the Creative Commons Attribution International License (CC BY 4.0).

<http://creativecommons.org/licenses/by/4.0/>



Open Access

Abstract

At present, there are relevant scientific materials on the cellular and molecular mechanisms of electrogenic Na/K pump function and structure, as well as on the potential- and ligand-activated ionic channels in the membrane. However, the role of electrogenic Na/K pump in regulation of semipermeable properties of cell membrane has not been elucidated yet, which is due to the fact that our knowledge about the biophysical properties of cell membrane is based on the conductive membrane theory of Hodgkin-Huxley-Katz, which is developed on internally perfused squid axon and lacks intracellular metabolism. Thus, the accumulated abundance of data on the role of G-proteins-dependent intracellular signaling system in regulation of Na/K pump activity and biophysical properties of cell membrane presumes fundamental revision of some statements of membrane theory. The aim of the present review is to briefly demonstrate our and literature data on cell hydration-induced auto-regulation of Na/K pump as well as on its role in metabolic control of semipermeable properties and excitability of neuronal membrane, which are omitted in the study of internally perfused squid axon.

Keywords

Na/K Pump, Hydration, Ionic Channel, Membrane, Na/Ca Exchange, Cyclic Nucleotides

1. Introduction

According to the classical membrane theory, which is developed by Nobel laureates Hodgkin, Huxley and Katz and concerns the ionic mechanisms involved in excitation and inhibition of cell membrane, the signal transmission in cells is

realized by potential- and agonist-activated ionic channels in membrane, while the Na/K pump, functioning in electro-neutral regime, has a housekeeping role in controlling the intracellular ionic homeostasis [1] [2]. The main failure of this theory is that it does not evaluate the role of intracellular metabolism in regulation of membrane excitability, namely it is unable to explain what mechanism controls low Na⁺ and high K⁺ permeability of cell membrane in resting state of neurons. This omission is due to the fact that the theory was initially developed on the basis of experimental data obtained by the study of internally perfused squid axon [1].

In 1957 Jens Christian Skou disclosed Na/K-ATPase as an enzyme and a working molecule of Na/K pump and characterized its biochemical and pharmacological properties [3]. Thus, the Na/K pump became a subject of various biochemical and biophysical studies resulting in a discovery that it functions in stoichiometry of 3Na:2K, which identifies the electrogenic character of pump. The historical aspects of this discovery are presented in the excellent review by Rogers Thomas [4], who was the first to elucidate the electrogenic character of Na/K pump in neurons by measuring and characterizing the membrane current generated by Na/K pump by means of combination of “voltage-clamp” and “intracellular selective microelectrode” methods in Prof. Gerald Kerkut’s laboratory [5] [6].

Although, at present the electrogenic character of Na/K pump can be considered as a proven fact, its multifunctional physiological role in regulation of biophysical properties of cell membrane, namely in controlling semipermeable properties of cell membrane, needs further evaluation. The problem of the functional role of Na/K pump in metabolic regulation of cell membrane function has served as one of the main research subjects of my group for more than 50 years. Thus, we have been able to solve some problems regarding the role of Na/K pump in metabolic regulation of semipermeable properties, excitability and chemosensitivity of neuronal membrane, which are briefly presented below.

2. The Na/K Pump Controls Membrane Potential in Neurons

The low and high permeability of cell membrane for Na⁺ and K⁺, respectively, are the main statements for membrane theory developed by Hodgkin-Huxley-Katz and are based on Goldman’s constant field theory suggesting that the membrane potential (MP) is a sum of electrochemical potentials for K (E_k), Na (E_{Na}) and Cl (E_{Cl}) ions. This is known as Goldman-Hodgkin-Katz equation:

$$V_m = \frac{RT}{F} \ln \left(\frac{P_K [K^+]_o + P_{Na} [Na^+]_o + P_{Cl} [Cl^-]_i}{P_K [K^+]_i + P_{Na} [Na^+]_i + P_{Cl} [Cl^-]_o} \right)$$

V_m is the MP, R is the universal gas constant, T is the temperature, F is the Faraday’s constant, P_K , P_{Na} and P_{Cl} are the membrane permeability for these ions. The symbols $[]_i$ and $[]_o$ refer to the thermodynamic activities of the ions depending on their being inside or outside of the cell, respectively.

However, the unreliability of this equation is shown by the study of MP dependence on $[K]_o$ and temperature. The studies on various objects have shown the absence of a linear dependence between MP and $[K]_o$ at low ranges up to 15 - 20 mM [4] [5].

The issue on MP deviation from the theoretical size of electrochemical potential (E_K) (calculated by Nernst formula at low $[K]_o$) became a subject of special considerations and a number of hypotheses on the nature of such a non-linear dependence between the MP size and $[K]_o$ were suggested [4]. However, none of them could give a reliable explanation of this phenomenon as well as evaluate the nature of the metabolic mechanism controlling potassium-electrode properties of cell membrane. In 1940 Dean theoretically suggested that the non-linear dependence of MP on $[K]_o$ could be an active extrusion of Na^+ from the cells [4]. This prediction of Dean was experimentally proven by Grundfest's study of MP dependence on $[K]_i$ in squid axon, demonstrating that the increase of $[K]_i$ did not lead to elevation of MP as was assumed by Nernst's law. Therefore, he noted the contribution of Na/K pump in generation of MP in axon [7]. However, as squid axon has high electrical conductivity, shunting the Na/K pump current and generating low MP value, the validity of these data has not been adequately considered in literature. Later, Grundfest's results were proven by a number of works performed on muscles [4] and neurons [8] [9].

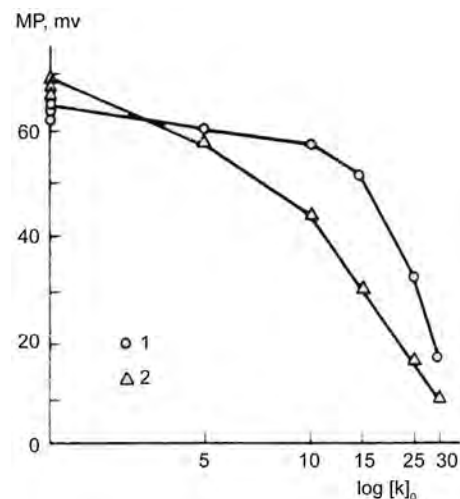


Figure 1. Membrane potential as a function of logarithm of external potassium ion concentration in “normal” Ringer’s solution (1) and in presence of 0.2 mM dinitrophenol (2) [8].

Our study regarding the dependence of ionic composition of snail neuron on $[K]_o$ has shown that the $[K]_o$ -induced decrease of $[Na]_i$, which takes place without changing $[K]_i$, as well as the activation of nerve ganglia respiration (O_2 uptake) are mostly expressed in the region of $[K]_o = 0 - 15$ mM, which is blocked by cold ($4^\circ C$) and Na/K pump inhibitor-strophanthin (Figure 1). This clearly indicates that in normal living state cell metabolism controls the level of MP through electrogenic Na/K pump [10].

By using the “voltage-clamp” and “concentration-clamp” methods we have shown that the 1mM $[K]_o$ with “0” effect on E_k , generates the potential-independent pump current in neurons, which proves that the $[K]_o$ -induced activation of pump is not due to membrane depolarization but is a result of $[K]_o$ -induced activation of Na/K-ATPase (**Figure 2**) [11].

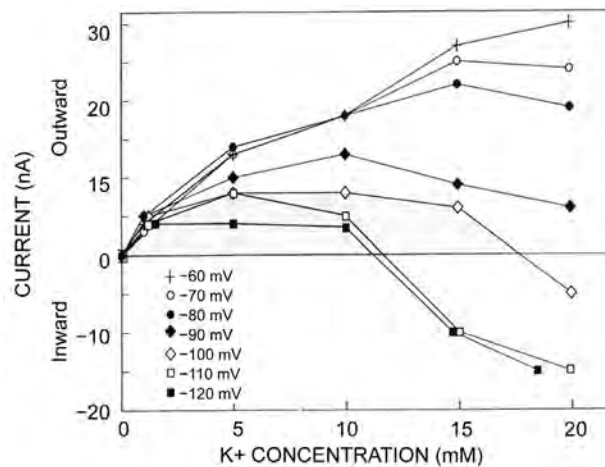


Figure 2. The MP-dependence of 1 mM $[K]_o$ -activated Na/K pump currents, which was measured by “voltage-clamp” and “concentration-clamp” methods [11].

The existence of Na/K pump-dependent component of MP was also demonstrated by a number of studies on the temperature sensitivity of cells MP. The incomparably higher temperature sensitivity of Na/K pump-dependent component of MP compared with E_k predicted from Nernst’s law (1.8 mV/10°C), has been shown in molluscan neurons having strong modulation effects on endogenous (pacemaker) activity [9] [12] [13] [14]. It has been shown that the variations of metabolic components of MP are responsible for the endogenous generation of electrical activity and spontaneous inhibition of this activity [13] [15].

3. The Dependence of Cell Volume on Na/K Pump Electrogenicity

At present, when the electrogenic character of Na/K pump is a well-documented fact, its central role in cell volume regulation has become more obvious. The evolution of the studies on the role of Na/K pump in cell volume regulation has recently been presented in an excellent review by Alan R. Kay and Mordecai Blaustein [16]. The second author of this work, during 50 years of his research, has published a number of pioneer discoveries regarding the carrier-driven ion transporting mechanisms, such as Na/K pump and Na/Ca exchange in membrane and their physiological meaning. However, the feedback mechanisms between cell volume and Na/K pump activity, as well as the role of Na/K pump-dependence on cell volume in regulation of biophysical properties of cell membrane, such as membrane permeability, fluidity, excitability and chemosensitivity remain non-sufficiently evaluated.

Since the rigidity of animal cell membrane is not so high to be able to stand to considerable gradients of both hydrostatic and osmotic pressures they behave as an osmometer: cell swells or shrinks by taking in or giving out water through the cell membrane. Therefore, for studying the dependence of Na/K pump activity on cell volume as well as the role of Na/K pump-dependent cell volume in regulation of membrane biophysical properties we have studied cell swelling and shrinkage in hypotonic and hypertonic saline, respectively. Neurons were chosen as experimental models because they have weak, expressed and fast cell volume recovery (CVR) systems to response of osmolality changes in cell bathing solution like non-excitabile cells [17].

The studies on the osmotic properties of isolated giant neurons of *Helix* and *Aplysia* mollusks have shown that the cell volume changes (swelling and shrinkage) to osmotic pressure have a discreet character [18] [19]. Such a non-gradual dependence of cell volume on osmotic gradients on the membrane has been explained by the existence of invaginations (caveolae) in cell membrane surface, which open by swelling and close by cell shrinking. The existence of caveolae in plasma membrane was identified by electron microscopy in 1953 [20], but their functions became a subject for investigations only at the end of the last century [21].

We have developed a system using cultured *Aplysia* neurons and confocal scanning laser microscopy to directly monitor cell volume when the osmolality of the perfusion solution is altered and when sodium transport is blocked. Volume changes of greater than 30% were observed, accompanied by changes in surface area of greater than 15%. The volume increases secondary to sodium pump inhibition and hypotonic solutions and the volume decrease secondary to hypertonic solutions were reversible. These results demonstrate that neuronal volume may change dramatically and raise the possibility that dynamic changes in neuronal cell volume may have physiological importance (Figure 3) [19].



Figure 3. The effect of 10^{-5} M ouabain containing ASW on medium neuron of *Aplysia*. The left neuron was in normal state, the right one was subjected to ouabain containing ASW for 5 min. Changes of neuronal volume of 30% or more were regularly observed with this manipulation and corresponding changes of surface are of at least 15% [19].

Although the electrogenic character of Na/K pump predicts its crucial role in cell volume regulation and it has been reported that such swelling occurs when Na/K pump is inhibited with cardiac glycosides and K-free solution, the existing data on this question are, to some extent, conflicting. The ouabain-induced pump inactivation in *in vitro* experiments isn't often accompanied by neuron swelling as it is predicted by pump hypothesis [16].

The detailed investigation of ouabain effect on water and ion contents of freshly prepared rabbit and rat renal cortical slices [22] [23] and isolated single neurons of mollusk [24] shows that the ouabain-induced pump inhibition is accompanied by cell swelling. The result is explained by the fact that cell membrane in fresh preparation has comparably higher electrical resistance, which brings to higher Na/K pump electrogenicity, while cells in "non-fresh" preparations are in their swelling state and pump electrogenicity is shunted, thus the ouabain-induced cell swelling is absent [23] [24]. It has been shown that the cell volume dependence on electrogenic Na/K pump activity is depressed by high membrane permeability for Cl ions, which increases as a result of the impairments of metabolic water efflux from the cell [24].

The normal Ringer used had the following composition: NaCl, 80 mM; KCl, 4 mM; CaCl₂, 7 mM; MgCl₂, 13 mM; Tris-chloride (pH 7.8), 10 mM; and glucose, 10mM. The potassium-free solution had an excess of 4 mM NaCl above normal. In order to change the tonicity (T ;) without altering the ionic strength, the NaCl content of the standard solution was reduced to 40 mM ($[Na]_o = 40 \text{ mM/}$) and sucrose was used to obtain media of different tonicities, from T , - 0.5 (0 mM sucrose) to T , - 2 (189 mM sucrose). In some experiments T , was equal to 2.5 (252 mM sucrose). In replacing NaCl by sucrose, 1 mM of NaCl was taken as osmotically equivalent to 1.57 mM of sucrose [25].

The fact that the electrogenicity of Na/K pump strongly depends on cell membrane resistance is indicated in the data presented in **Figure 4** on the membrane I-V characteristics and Na/K pump current (I_p) depending on osmolality of cell bathing PS, where the peak of I_p after the transfer of neurons from K-free to normal PS is increased with a rise in tonicity, which is accompanied by the increase of membrane resistance.

Thus, the obtained data indicate that there is a negative feedback between Na/K pump-generated currents and membrane permeability that is realized by Na/K pump-activated cell shrinkage, which has a crucial role for the quick recovery of the factor-induced increase of membrane permeability [18].

4. The Na/K Pump Controls Membrane Semipermeability and Excitability

One of the essential omissions of membrane theory of Hodgkin-Huxley-Katz on nerve excitation is the disregard of water fluxes through the membrane, which are potential-dependent and lead to cell volume changes. Although, from the thermodynamic point of view, it is predicted that the MP variation leads to respective changes of osmotic gradient on the membrane by generating water

fluxes through the membrane and cell volume changes. It is worth noting that one of the main postulates of membrane theory is that “membrane conductance increases by membrane depolarization”, but the role of water influx through the membrane in determining membrane depolarization-induced increase of membrane conductance has not been considered [1]. Meanwhile, Tasaki and co-workers [26], as well as Terakawa [27] have shown that membrane depolarization and hyperpolarization lead to axon swelling and shrinkage, respectively, even during generation of single action potential by using the elegant experimental methods for detection of squid axon diameter changes.

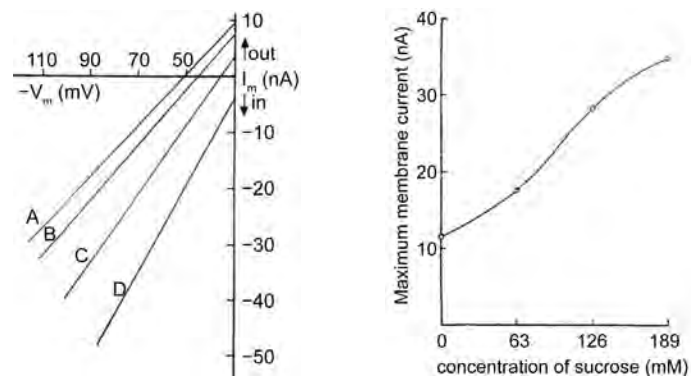


Figure 4. The I-V characteristics of membrane and peak of pump-induced current in normal Ringer's solutions with different tonicities after preliminary incubation of neurons in potassium-free solution. The cell was clamped at the resting potential level in normal Ringer's Motion (46 mV). The curve was drawn by eye [18].

Although at present the role of electrogenic Na/K pump as a powerful mechanism in controlling water fluxes through the membrane and the cell volume can be considered as a well-documented fact, the physiological meaning of such fundamental properties of Na/K pump has not been adequately considered in literature. Therefore, this question was the subject of our study [28].

It is known that Na/K pump generates water efflux from the cells due to its function in stoichiometry of 3N:2K and, being the highest APT utilizing machine in membrane, it stimulates endogenous water molecules during intracellular oxidative-phosphorylation.

Traditionally, the role of electrogenic Na/K pump in regulation of membrane excitability is explained by pump-induced membrane hyperpolarization. However, as can be seen in the studies on the neuronal endogenous activity of Japanese land snail presented in Figure 5, in case of the Na/K pump inactivation by K-free physiological saline the membrane hyperpolarization is accompanied by activation of electrical activity of neuron, while at 5mM $[K]_o$ -induced activation of pump, the membrane depolarization is accompanied by inhibition of its activity [28].

The potential-independent and Na/K pump-induced inhibition of neuronal activity is more pronounced when $[K]_o$ is replaced by $[Rb]_o$. The analogical depression has been obtained by noradrenalin-induced activation of Na/K pump as

well as by applying hypertonic solution [28].

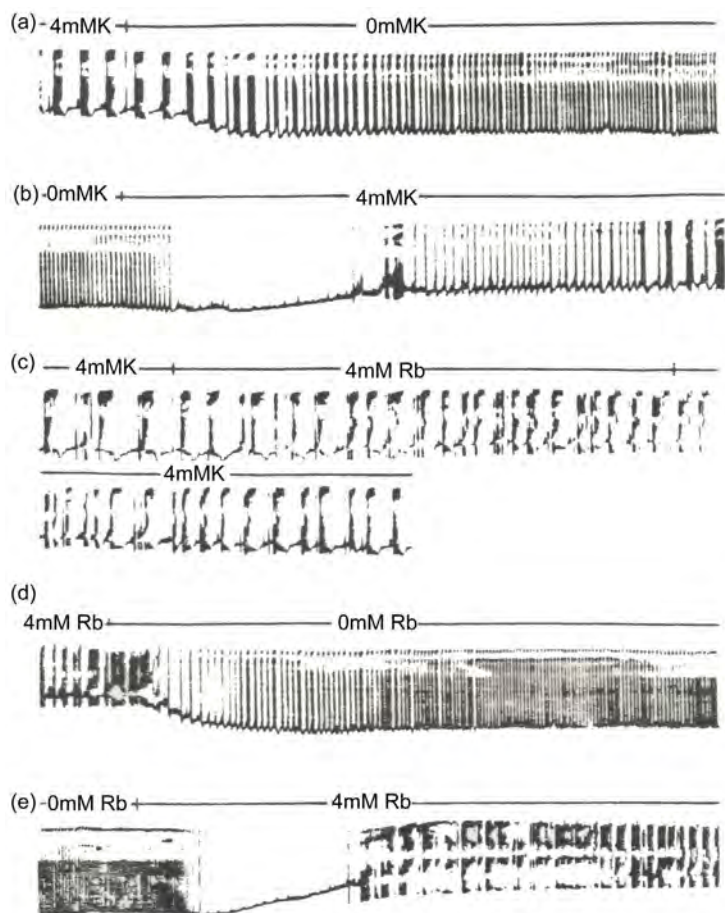


Figure 5. The effect of 0 mM K (a), 4 mM K (b), 0 RbmM (d) and 4 mM Rb (e) induced hyperpolarization and 4 mM K replacement by 4 mM Rb (c) in external solution on bursting activity of pacemaker neurons [28].

Thus, the obtained data clearly indicate that the Na/K pump-induced inactivation of membrane excitability is also realized by potential-independent mechanism, which can be due to water efflux and membrane surface decrease as a result of cell shrinkage. For estimation of the role of water fluxes through membrane in regulation of membrane excitability, the effect of hypertonic solution-induced water efflux on membrane inward sodium (I_{Na}) and outward potassium (I_K) currents in internally perfused squid axon as well as in intracellular perfused and intact neurons has been studied [29] [30] [31].

The method of internal perfusion of giant axon is similar to the method of Baker *et al.* [32]. The control isotonic solution for the axons contains (in mM): NaCl 517, KCl 5; $CaCl_2$ 50; Na-HEPES (pH 7.8) 12.7. A solution with low Na concentration is prepared by replacing 300 mM NaCl by 500 mM glucose. The isotonic internal solution contains (in mM) KF 100, glucose 888, Na-HEPES 12. Hypertonic and hypotonic solutions are prepared by adding or reducing 500 mM glucose in corresponding isotonic solutions.

As can be seen in **Figure 6**, water efflux has time-dependent activation of potassium currents (I_k) and depressed tail currents are due to I_k [33].

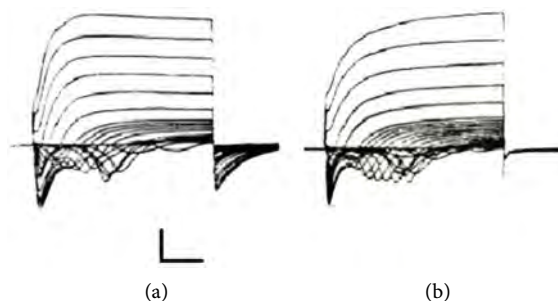


Figure 6. (a) Transmembrane ionic currents in internally perfused squid axon when in both sides of the membrane there were isotonic solutions; (b) Transmembrane ionic currents in internally perfused axon when it was internally hypotonic and externally isotonic solutions (outward water fluxes). The calibrations are 25 nA and 10 msec [33].

It is known that TTX (specific inhibitor for Na channels) in 10^{-9} M fully inhibits Na channels which are in active state. In order to evaluate the inactivation and activation effects of water efflux and influx on inward Na current, respectively, we have studied the effects of water influx on excitability of the axon poisoned by 10^{-8} M TTX, *i.e.* where all active Na channels are in blocked states.

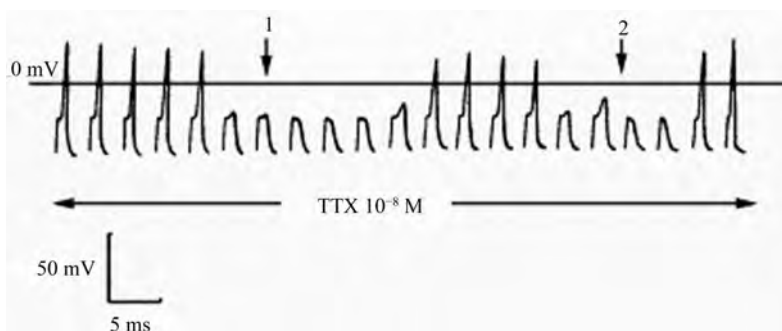


Figure 7. The transient recovery of the action potentials in squid giant axon in 10^{-8} M TTX containing solution at changes of the tonicity of the external solution. Originally the axon was perfused by the hypertonic external and isotonic internal solutions (outward transmembrane water flow was present). At the first arrow the outside hypertonic solution was replaced by isotonic one (transmembrane water flow was stopped). At the second arrow, external isotonic solution was replaced by the hypotonic one and inward transmembrane water flow was present. Outward and inward transmembrane water flows were produced by adding or removing 500 mM glucose in external isotonic solution [29].

As can be seen in **Figure 7**, the transient recovery of the action potentials was observed in 10^{-8} M TTX-containing solution, when water influx through the membrane was applied. These data clearly indicate that there are Na channels in axon with different energy activations and water influx has activation effects on

“reserve” channels, which are poisoned only by their activation. These suggestions are supported by the data of “voltage-clamp” study on water inward and outward water fluxes effects on inward I_{Na} and outward I_K in internally perfused squid axon in normal (517 mM NaCl) and 217 mM NaCl external solution (Figure 8).

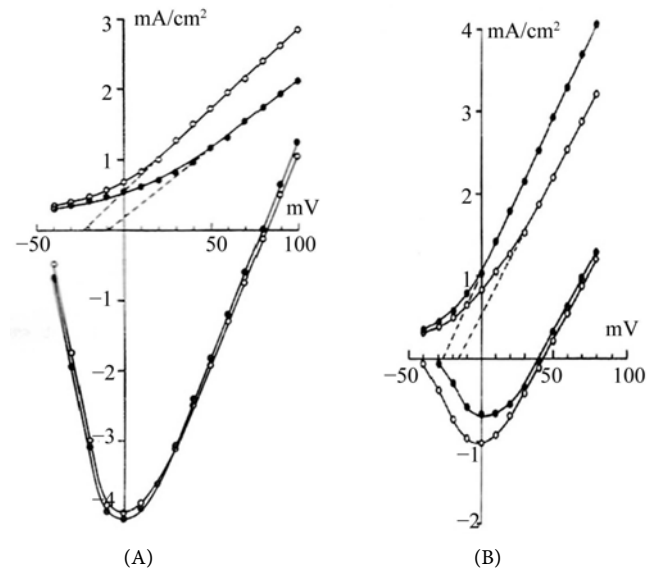


Figure 8. (A) Voltage of the membrane with (A) and without (B) inward water flow at the normal $[Na]_o = 517$ mM NaCl. The peak of inward and steady outward currents at the end of 25-msec depolarizing voltage pulses with (o) and without (.) the water flow as plotted against the membrane potential. The holding potential was -100 mV. (B) Current-Voltage relations the membrane currents with and without outward water flow at the $[Na]_o = 217$ mM NaCl [29].

As can be seen in Figure 8, water efflux has activation effect on potassium outward current (I_k) but has no significant effect on inward current (I_{Na}) at external medium containing 517 mM NaCl, *i.e.*, where Na gradient has stronger effect on channel than water efflux from the axon (A), while at low (217 mM) NaCl external solution the water influx has inactivation effect on I_k and significant activation effect on I_{Na} (B). These data indicate that water fluxes have activation effect on ionic currents having the same direction and inactivation effect on the ionic currents with opposite directions [29]. The fact that the number of functionally active channels depends on the membrane surface changes is clearly demonstrated by the study of ionic currents in snail intact neurons incubated in physiological solution (PS) with different osmolality [29].

As can be seen in Figure 9, upon the addition of 252 mM sucrose to the external solution, the volume of snail neurons gradually diminishes for 10 - 20 min and then stabilizes, *i.e.* for about 10 min the outward water flow through the membrane takes place and then stops after stabilization of the cell volume. Upon the returning of the neuron to the isotonic medium, the opposite process, in-

ward water flow through the membrane takes place [18] [29]. The study of the same time-dependent changes of amplitudes of outward K currents shows that, beginning from the 30th sec after placing the neuron in the hypertonic solution, the K outward current increases despite the fact that the amplitude of the command pulse remains constant. After 2.5 min, the outward current reaches its maximum value and then begins to decrease. Such a decrease of the K current lasts up to the 10th min, *i.e.* until stabilization of the neuronal volume in the hypertonic solution [18] [29].

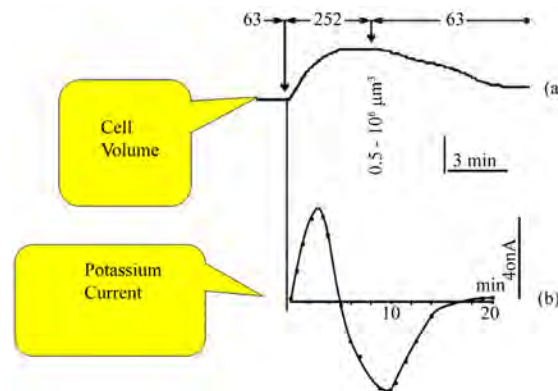


Figure 9. Time-dependent changes of cell volume and amplitudes of potassium currents after replacing isotonic PS by hypertonic (252 mM sucrose) and after returning of the neuron to the isotonic medium [18] [29].

The theoretical analysis of the experimental data on the effect of the outward and inward water flows on the outward potassium currents showed the maximum potassium conductance (G_{kmax}) increases by outward water efflux, while the inward water flow has the opposite effect. These data suggest that the changes of transmembrane currents during transmembrane water flow in dialyzed neurons are mainly due to the changes in single-channel conductance and the time constant of current activation [31].

Thus, the presented data firstly elucidate the nature of the metabolic mechanism controlling low permeability of cell membrane for Na and high permeability for K ions: osmotic water influx precedes the activation of sodium ionic channels for inward currents. Therefore, the metabolic water efflux from the cell, in which Na/K pump has a central role, inactivates membrane permeability for Na influx and activates membrane permeability for K efflux. Thus, on the basis of the aforementioned data, the impairment of Na/K pump-induced water efflux from the neurons, leading to the increase of membrane permeability for Na and membrane excitability, is suggested as a common consequence of nerve disorders.

5. The Na/K Pump Dependence on Cell Volume: The Auto-Regulation of Na/K Pump

As the electrogenic Na/K pump has a pivotal role in cell volume regulation, it is

predicted to be a negative feedback between cell volume and Na/K pump activity through which the auto-regulation of Na/K pump takes place. To check this suggestion we have studied the dependence of Na/K pump activity on cell volume by changing the osmolality of cell surrounding medium by means of measuring ^{22}Na efflux from the cells and counting pump units (^3H -ouabain receptors) in membrane [18].

The information about the osmolality effects on Na/K pump activity in the literature is contradictory: Keynes (1965) has observed that an increase in external tonicity stimulates the active ^{22}Na efflux from muscle [34], Mullins and Awad [35] haven't observed significant effect of tonicity on ^{22}Na efflux, while Venosa has shown that the tonicity leads to stimulation of ^{22}Na from muscle [36]. We have studied the dependence of cell bathing medium tonicity on ^{22}Na efflux from neurons with low and high $[\text{Na}]_i$. For this purpose, before ^{22}Na efflux measurement in normal saline with different osmolality, the neurons were incubated in K-free, ^{22}Na containing medium for 15 min (in case of low $[\text{Na}]_i$) and for 6 hours (in case of high $[\text{Na}]_i$). As can be seen in **Figure 10**, cell shrinkage activates the ^{22}Na efflux at low $[\text{Na}]_i$ and inhibits it at high $[\text{Na}]_i$.

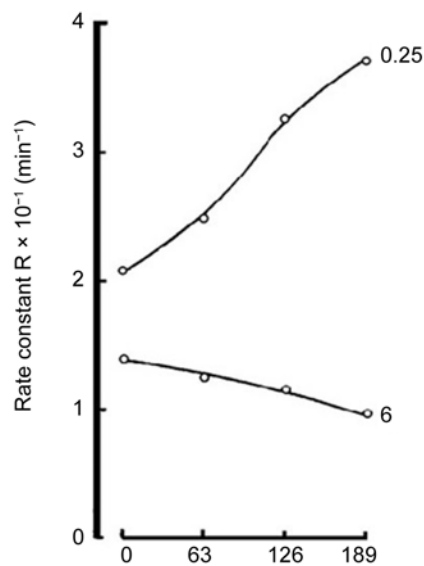


Figure 10. The initial rate constant of ^{22}Na efflux from the cells and the number of ^3H -ouabain molecules binding with membrane as a function of the tonicity of the surrounding medium for cells exposures for 25 min and 6 hours to cold K-free solution containing of ^{22}Na . Numbers on the right-hand side of the curves represent the incubation times (hours). Curves are drawn by eye [18].

By this study it becomes clear that osmolality increase of cell bathing solution has double effects on Na/K pump activity: on one hand it activates Na/K pump by shrinkage-induced increase of $[\text{Na}]_i$ and on the other hand it decreases pump activity by an unknown mechanism in case of high $[\text{Na}]_i$. The double effect of osmolality on cell surrounding medium on Na/K pump activity is more clearly

demonstrated by the study on the dependence of the rate constant of Na efflux from neurons on time in solutions with different tonicities.

In order to determine whether the number of functioning pump units in the membrane is changed in response to dependent changes of cell volume the inhibitory effect of ouabain on Na/K pump activity as well as [^3H]-ouabain binding with cell membrane of bathing neurons with different osmolality have been studied.

Table 1. Binding of [^3H]-ouabain to *Helix pomatia* cell membrane as a function of concentration of glycoside in solutions with different tonicities ($\times 10^8$ molecules/mg dry weight) [18].

Ouabain Content (Mol)	Incubation Medium		
	Hypotonic	Isotonic	Hypertonic
10×10^{-10}	4.59 ± 0.32	3.23 ± 0.24	2.03 ± 0.16
3×10^{-10}	18.3 ± 1.4	11.7 ± 0.87	6.29 ± 0.41
6×10^{-10}	28.9 ± 2.0	17.9 ± 1.2	10.0 ± 0.67
1×10^{-9}	32.0 ± 2.2	21.1 ± 1.4	12.2 ± 0.9
3×10^{-9}	144 ± 29.4	90.5 ± 5.7	53.8 ± 3.1
6×10^{-9}	431 ± 29.4	266 ± 15.8	147 ± 9.7
1×10^{-8}	793 ± 45.6	508 ± 30.1	283 ± 19.4

The data presented in **Table 1**, clearly indicate that cell swelling in hypotonic medium increases the number of ouabain receptors in membrane, while the shrinkage in hypertonic solution leads to opposite effects, *i.e.* to the decrease of the number of ouabain receptors compared with the number of ouabain receptors of neurons bathing in isotonic medium.

To elucidate whether the number of functioning pump units is changed under normal conditions in response to the increased passive membrane permeability, the binding of [^3H]-ouabain to the membrane was studied in the presence of synaptic transmitters [18].

Table 2. The effects of Ach, GABA and PTZ on [^3H]-ouabain binding to neuronal membrane [18].

Ouabain Content in the medium (Mol)	Normal Ringer	Normal Ringer Containing 10^{-4} M Ach	Normal Ringer Containing 10^{-4} MGABA	Isotonic + 5×10^{-2} M PTZ
10×10^{-20}	3.16 ± 0.48	5.13 ± 0.62	4.24 ± 0.21	5.21 ± 0.28
1×10^{-9}	20.56 ± 0.55	30.54 ± 1.55	27.63 ± 3.17	17.18 ± 1.1
5×10^{-9}	109.40 ± 10.47	170.29 ± 13.36	139.62 ± 11.43	26.79 ± 1.8
1×10^{-8}	143.54 ± 8.91	270.93 ± 28.53	174.48 ± 13.54	29.0 ± 2.3
1×10^{-7}	3254.47 ± 74.20	3944.33 ± 107.23	-	-
1×10^{-6}	23938.20 ± 852.41	3944.33 ± 107.23	-	-

From **Table 2**, it can be clearly seen that ACh and GABA increase ouabain binding significantly. Therefore, we suggest that the increased membrane permeability brought about by exposure to synaptic transmitters is accompanied by a corresponding alteration in the number of functioning pump units in the membrane.

Thus, the facts that water influx leads to the increase of membrane permeability for ions leading to cell swelling, which stimulates the pump activity by the increase of the number of pump units in membrane, while the pump activation-induced cell shrinkage decreases membrane permeability (membrane conductance) and the number of pump units in membrane, indicate that pump-dependent cell volume serves as an auto-regulatory system for pump. By this mechanism the metabolic regulation of membrane functions, such as excitability [37], chemo-sensitivity [38] [39] and second exchanger systems are realized. Therefore, the dysfunction of the auto-regulation of Na/K pump is suggested as a common consequence of cell pathology.

6. The Ouabain Inactivates Na/K Pump and Activates Na/Ca Exchange

Baker *et al.* have identified two components of ^{22}Na efflux in intra-perfused squid axon. They are ouabain-sensitive and insensitive components, which are due to Na/K pump and Na/Ca exchange in reverse (R) mode, respectively [40]. These authors, have explained the activation of R Na/Ca exchange by Na/K pump inactivation-induced increase of $[\text{Na}]_i$. Our study of dose-dependent ouabain effect on ^{22}Na efflux from intact neurons and rat brain and heart muscle tissues has shown that ouabain inactivates Na/K pump only at high ($>10^{-7}$ M) concentrations, while the low concentrations ($<10^{-7}$ M) of ouabain have activation effects on ^{22}Na efflux from the cells (**Figure 11**), which does not have effect on Na/K pump activity measured by ^{86}Rb uptake (**Figure 12**).

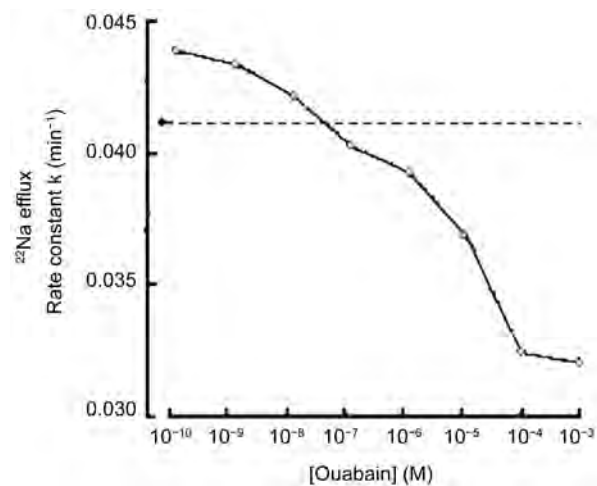


Figure 11. The dose-dependent (10^{-10} to 10^{-3} M) ouabain effect on the rate constant of ^{22}Na efflux from the neurons [18].

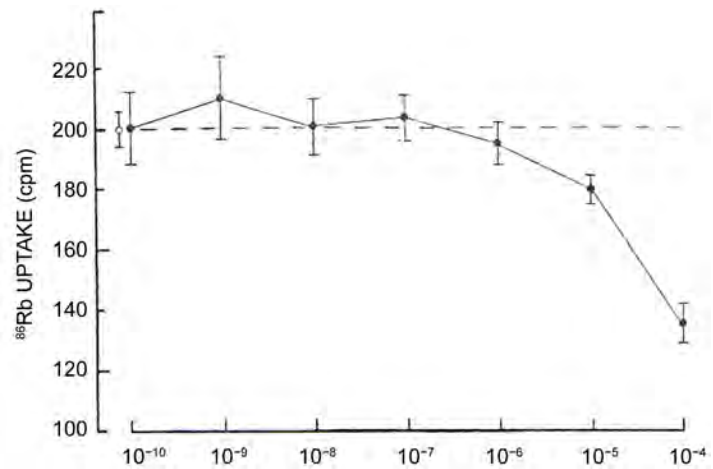


Figure 12. The dose-dependent (10^{-10} to 10^{-3} M) ouabain effect on the rate constant of ^{86}Rb uptake in neurons [43].

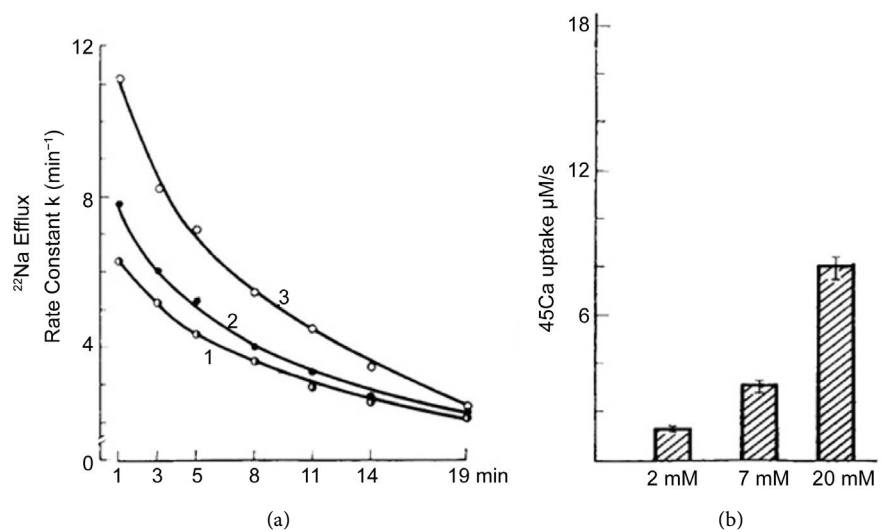


Figure 13. (a) The time-dependent ^{22}Na efflux from the neurons in presence of 2 mM (1); 7 mM (2) and 20 mM (3) Ca; (b) ^{45}Ca -uptake by neurons at 2 mM; 7 mM and 20 mM Ca [43].

It has been shown that activation of ^{22}Na efflux by low ouabain in intact neurons, like ouabain-insensitive ^{22}Na efflux in perfused axon [40], is due to activation of R Na/Ca exchange (**Figure 13(a)** and **Figure 13(b)**). The ^{22}Na efflux from neurons in K-free solution is activated by the increase of Ca content in cell bathing medium (**Figure 13(a)**), which is accompanied by ^{45}Ca uptake increase (**Figure 13(b)**).

In order to evaluate how the dose-dependent effect of ouabain on ^{22}Na efflux is related with ouabain binding with membrane receptors we have studied the dose-dependent [^3H]-ouabain binding with cell membrane of snail neurons.

It has been shown that two saturated components of ouabain binding may be distinguished on the dose-dependent curve of ouabain binding with cell membrane: one—at concentrations from 10^{-10} to 10^{-9} M and the other—at ouabain

concentrations between 10^{-9} and 10^{-7} M. Moreover, the kinetics of dose-dependent ouabain binding curve does not change by variation of osmolality of cell bathing medium (Figure 14) [18].

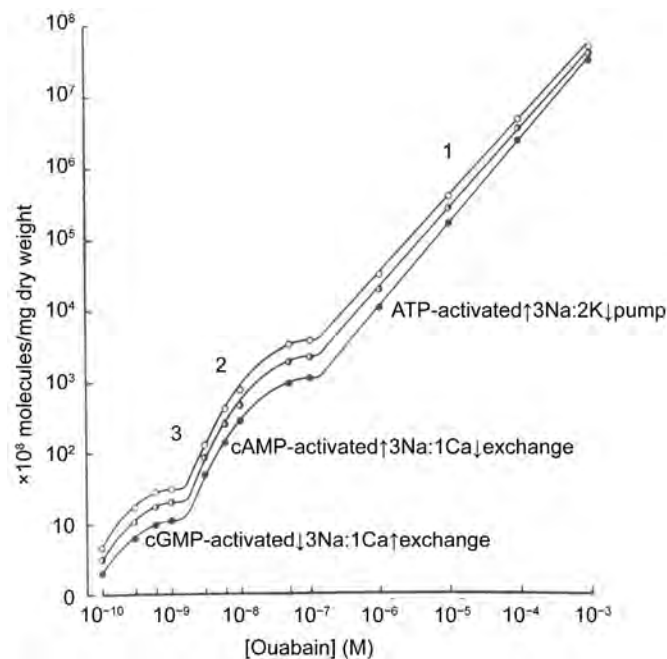


Figure 14. Dose-dependent [^3H]-ouabain binding with cell membrane in isotonic, hypertonic and hypotonic mediums [18].

Later, these three types of ouabain receptors were characterized as α_1 , α_2 and α_3 isoforms of Na/K-ATPase [41]. The involvement of these receptors in R Na/Ca exchange was explained by ouabain-induced inactivation of Na/K pump leading to local increase of $[\text{Na}]_i$ [42].

However, our study on mollusk neurons, rat brain and heart muscle tissues has shown that the function of low ouabain-induced activation of Na/Ca exchange and the function of α_2 and α_3 receptors has no direct relation with Na/K pump activity [43]. It has been shown that the activation of Na efflux from the cells by both $[\text{cGMP}]_i$ and $[\text{cAMP}]_i$ are due to Na/Ca exchange in forward mode (F) and R Na/Ca exchange, respectively. The activation of α_3 and α_2 receptors stimulates the cGMP-dependent F Na/Ca exchange, and cAMP-dependent R Na/Ca exchange, respectively [43] [44].

It has also been shown that α_3/α_2 receptors are non-specific for ouabain molecules and serve as common membrane targets for the impact of various weak chemical and physical signals unable to activate ionic channels and Na/K pump activity such as low concentrations of transmitters ($<10^{-12}$ M) [45] [46], magnetized solution, microwave having intensity even less than the thermal thresholds [47] [48].

Figure 15 shows that low concentration of Ach, which is unable to activate ionic channels and Na/K pump activity in neurons, has potential-independent

modulation of GABA-induced ionic currents in neuron, while in oocytes injected with mRNA for different receptors this modulation is absent (Figure 15). These data clearly indicate that low Ach effect on GABA-induced current is not realized through Ach receptor or Na/K pump, and is due to activation of cAMP-dependent activation of R Na/Ca exchange [46].

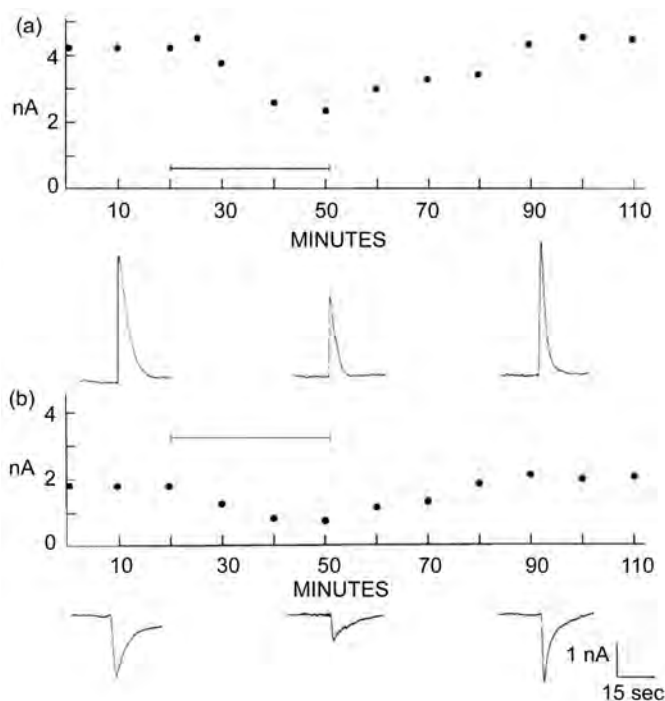


Figure 15. The effect of 10^{-13} M Ach (applied during the bars from 20 to 50 min) on GABA responses of a medial pleural neuron. Part A shows a plot of peak GABA response amplitude with time when the neuron was held at -50 mV. Three records of the currents are shown below the plot to illustrate the control, depressed, and recovered GABA currents. After microperfusion of Ach the peak amplitude declined to about 40% of control. Part B shows results of a repeat of this experiment in the same neuron, but with the holding potential at -65 mV [46].

The extra-sensitivity of α_3/α_2 receptors in membrane to various factors is in harmony with the groundbreaking discoveries of Robert Lefkowitz and Brian Kobilka regarding the extremely sensitive G-proteins-coupled receptors in cell membrane for which they have been awarded the Nobel Prize in Chemistry [49]. Thus, these data indicate that the high concentration of ouabain ($>10^{-6}$ M) can only be considered as a specific inhibitor for Na/K-ATPase [3], while the low concentrations of ouabain have only intra-signaling function, which is thoroughly described in the review by Xie and Askari [50] [51].

It is worth noting that activation of both cGMP-dependent F Na/Ca exchange and cAMP-dependent R Na/Ca exchange generates water efflux from the cell, decreases membrane permeability for Na ions and controls Na gradient on the membrane: the cGMP-activated F Na/Ca exchange stimulates Na/K pump by

removing $[Ca]_i$, generating water efflux from the cells and decreasing membrane permeability for Na ions, while cAMP-activated R Na/Ca exchange, stimulates endogenous water formation by $[Ca]_i$ -induced activation of mitochondrial function, which also generates water efflux from the cells and decreases membrane permeability for Na and controls Na gradient on the membrane. Thus, this explains the metabolic regulation of membrane semipermeability [44].

This suggestion is supported by the data on weak intensity static pulsing and magnetic field effects on cGMP-activation of F Na/Ca exchange in normal PS and activation of cAMP-dependent R Na/Ca exchange in K-free medium (Figure 16) [52] [53].

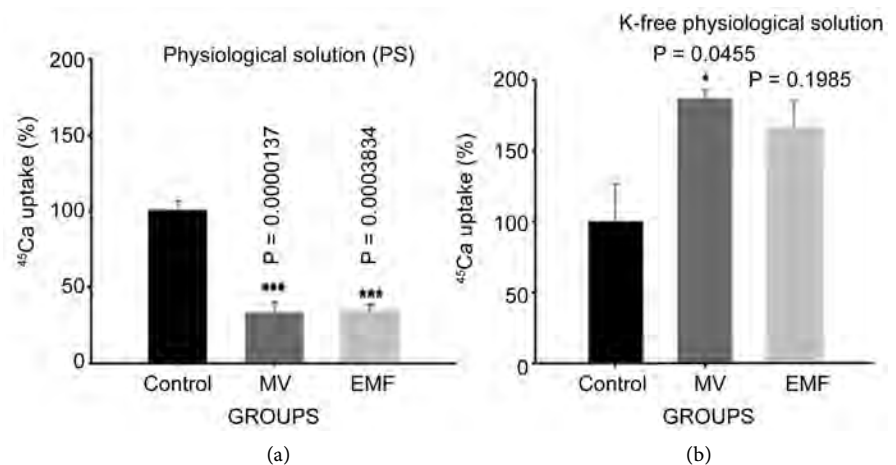


Figure 16. The effect of 4Hz mechanical vibration (MV) and ELF EMF on $^{45}Ca^{2+}$ uptake by neuronal ganglia in (a) normal PS and (b) K-free solution [53].

At present, the discovery of the role of intracellular cGMP/cAMP in regulation of Na/Ca exchange between cells and external medium as well as between different organoids and cytoplasm [54], allows to consider the extra-sensitivity of cyclic nucleotides-dependent changes of $[Ca]_i$ as a primary mechanism for modulation of Na/K pump activity in response to the impact of weak factors on cells and organism [55].

The study of synaptic transmitters sensitivity of cGMP-activated F Na/Ca exchange and cAMP-activated R Na/Ca exchange has shown that cGMP system is more sensitive to transmitters effects ($<10^{-15}$ M) than cAMP system (10^{-12} - 10^{-13} M) [56] [57].

On one hand the highest sensitivity of cGMP-dependent F Na/Ca exchange and on the other hand the high permeability of cell membrane for water allow us to suggest that the factor-induced cell hydration serves as a primary mechanism for the activation of soluble guanylate cyclase-induced cGMP synthesis. To check this suggestion, we have studied the effect of cell hydration on intracellular contents of cGMP and cAMP [56] [57]. It is known that membrane water permeability is elevated as a result of membrane fluidity increase. By our previous study we have shown that short chain fatty acids activate the membrane

fluidity, through which the strong modulation of membrane functions takes place [58] [59] [60].

Figure 17 shows that when K-free saline is added in cell bathing medium, non-metabolized 2-decenoic fatty acid (DA) leads to cell swelling, which is accompanied by the increase of cGMP without significant changes of cAMP contents. These data allow us to suggest that the increase of cell hydration could be a primary mechanism for activation of cGMP-dependent F Na/Ca exchange.

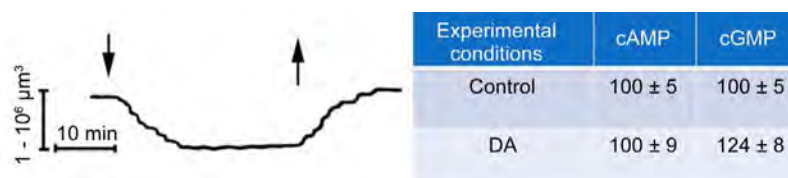


Figure 17. The 2-decenoic fatty acid-induced cell swelling in K-free solution. The first arrow indicates the moment when the K-free solution was replaced with K-free DA containing solution, the second arrow shows the moment of the effect of DA-induced water uptake on intracellular cyclic nucleotides (in %) [60].

Thus, the aforementioned data allow us to suggest that the dysfunction of cGMP/cAMP-dependent Na/Ca exchange-induced increase of $[Ca]_i$, which inhibits Na/K pump, is considered as a common consequence of cell pathology including cancer [61] [62] [63] [64], nerve disorders [65] [66] and cardio-vascular diseases [67] [68].

Although the Na/Ca exchange functions in stoichiometry of 3Na:1Ca [40], its activation in forward mode has hydration effect, while in reverse mode its activation has dehydration effect only on brain tissue of old animals, when $[Ca]_i$ is high. However, at low $[Ca]_i$ (in young animals), the activation of F Na/Ca exchange has dehydration effect on brain tissue as $[Ca]_i$ decrease leads to activation of Na/K pump, while the activation of RNa/Ca exchange leads to hydration of brain tissue by $[Ca]_i$ -induced activation of mitochondrial production of H_2O [44]. It is worth noting that in young animals the activation of both F Na/Ca and R Na/Ca exchanges stimulates water efflux from the cells, leading to the decrease of membrane permeability for Na, and Na efflux from the cells leads to the increase of Na gradient on membrane serving as energy sources for different secondary exchange systems. These data indicate that the Na/Ca exchange in both directions is a key protective cell mechanism, the dysfunction of which brings to cell pathology, including aging [65] [68].

7. Conclusions

- 1) The electrogenic Na/K pump generates metabolic components of membrane potential through which the control of potassium electrode properties predicted by Nernst's law is realized.
- 2) Unlike ionic gradient-induced membrane currents, the Na/K pump current is increased by the elevation of membrane resistance.
- 3) As Na/K pump functions in stoichiometry of 3Na:2K, and is the highest

ATP utilizing machine; it increases endogenous water formation by activation of oxidative phosphorylation and generates water efflux from the cells. The latter, besides balancing osmotic water influx, has a pivotal role in controlling semi-permeable properties of cell membrane in resting state of neuron, *i.e.* low permeability for Na and high permeability for K ions.

4) The Na/K pump activation decreases the number of functionally active Na channels in membrane by both surface-dependent decrease of the number of functionally active channels and water efflux-induced inactivation of these ionic channels. Thus, there is a negative feedback between the number of functionally active Na ionic channel in membrane and Na/K pump activity.

5) There is also a negative feedback between cell volume and Na/K pump activity, which is realized through surface-dependent changes in the number of Na/K pump units (ouabain receptors), through which the autoregulation of Na/K pump activity is realized.

6) In intact neurons the curve of dose-dependent ouabain binding with cell membrane consists of two saturated and one linear part, out of which low affinity receptors with linear dose-dependent character are identified by Na/K pump functions, while the high and middle affinity receptors have cGMP-dependent F Na/Ca exchange and cAMP-dependent R Na/Ca exchange functions, respectively.

7) The intact neurons, unlike in case of neurons in internally perfused axon, have low ouabain-activated Na efflux, which is due to cAMP-dependent R Na/Ca exchange. The activation of the latter also takes place upon the impact of various weak chemical and physical signals, which are unable to activate ionic channels and modulate Na/K pump activity. Thus, it is suggested that G-proteins in membrane serve as such common sensors which activate cGMP and cAMP contents in the cell.

8) The activation of both cGMP-dependent FNa/Ca exchange and cAMP-dependent R Na/Ca exchange generates water efflux from the cell, decreases membrane permeability for Na ions and controls Na gradient on the membrane. The cGMP-activated F Na/Ca exchange stimulates Na/K pump by removing $[Ca]_i$, generating water efflux from the cells and decreasing membrane permeability for Na ions, while cAMP-activated R Na/Ca exchange, stimulates endogenous water formation by activation of mitochondrial function, which also generates water efflux from the cells and decreases membrane permeability for Na and controls Na gradient on the membrane. Thus, this explains the metabolic regulation of membrane semi permeability.

9) The dysfunction of G-proteins-regulated GMP/cAMP-dependent Na/Ca exchange, which controls low level of $[Ca]_i$ and inhibits Na/K pump, is a common consequence of cell pathology.

Conflicts of Interest

The author declares no conflicts of interest regarding the publication of this paper.

References

- [1] Hodgkin, A.L. (1964) The Consecution of the Nervous Impulse. University Press, Liverpool.
- [2] Katz, B. (1966) Nerve, Muscle and Synapse. Raven Press, New York.
- [3] Skou, J.C. (1957) The Influence of Some Cations on an Adenosine Triphosphatase from Peripheral Nerves. *Biochimica et Biophysica Acta*, **23**, 394-401.
[https://doi.org/10.1016/0006-3002\(57\)90343-8](https://doi.org/10.1016/0006-3002(57)90343-8)
- [4] Thomas, R.C. (1972) Electrogenic Sodium Pump in Nerve and Muscle Cells. *Physiological Reviews*, **52**, 563-594. <https://doi.org/10.1152/physrev.1972.52.3.563>
- [5] Kerkut, G.A. and Thomas, R.C. (1965) An Electrogenic Sodium Pump in Snail Nerve Cells. *Comparative Biochemistry and Physiology*, **14**, 167-183.
[https://doi.org/10.1016/0010-406X\(65\)90017-4](https://doi.org/10.1016/0010-406X(65)90017-4)
- [6] Thomas, R.C. (1969) Membrane Current and Intracellular Sodium Changes in a Snail Neuron during Extrusion of Injected Sodium. *The Journal of Physiology*, **201**, 495-514. <https://doi.org/10.1113/jphysiol.1969.sp008769>
- [7] Grundfest, H., Kao, C.Y. and Mirano, M.A. (1954) Bioelectric Effect of Ions Micro-injected into the Giant Axon of Loligo. *Journal of General Physiology*, **38**, 245-282.
<https://doi.org/10.1085/jgp.38.2.245>
- [8] Ayrapetyan, S.N. (1969) Metabolically Dependent Fraction of Membrane Potential and Electrode Properties of the Membrane of Giant Neurons in Mollusks. *Biofizika*, **14**, 1027-1031.
- [9] Gorman, A.L. and Marmor, M.F. (1970) Contribution of Sodium Pump and Ionic Gradients to the Membrane Potential of Molluscan Neuron. *Physiology*, **210**, 897-917. <https://doi.org/10.1113/jphysiol.1970.sp009248>
- [10] Ayrapetyan, S.N., Nasarenko, A.R. and Sorokina, Z.A. (1970) Dependency of Active Ion Transport in Snail Neurons of Ionic Composition of Extracellular Medium. *Biofizika*, **16**, 1037-1042.
- [11] Ayrapetyan, G., Ayrapetyan, S. and Carpenter, D. (1991) The Electrogenic Sodium Pump Activity in Aplysia Neuron Is Not Potential-Dependent. *Acta Biologica Hungarica*, **50**, 27-34.
- [12] Carpenter, D.O. and Alving, B.O. (1968) A Contribution of an Electrogenic Na⁺ Pump to Membrane Potential in Aplysia Neurons. *Journal of General Physiology*, **52**, 1-21. <https://doi.org/10.1085/jgp.52.1.1>
- [13] Carpenter, D.O. (1970) Membrane Potential Produced Directly by the Na Pump in Aplysia Neurons. *Comparative Biochemistry and Physiology*, **35**, 371-385.
[https://doi.org/10.1016/0010-406X\(70\)90602-X](https://doi.org/10.1016/0010-406X(70)90602-X)
- [14] Ayrapetyan, S.N. (1969) Effect of Temperature on Membrane Potential of Giant Neurons in Snails. *Biofizika*, **14**, 663-668. <https://doi.org/10.1007/BF01124277>
- [15] Ayrapetyan, S.N. (1969) Mechanism of Regulation of Spontaneous Activity of Snail Giant Neurons. *Biofizika*, **14**, 866-872. (In Russian)
- [16] Kay, A.R. and Blaustein, M.P. (2019) Evolution of Our Understanding of Cell Volume Regulation by the Pump-Leak Mechanism. *Journal of General Physiology*, **151**, 407-416. <https://doi.org/10.1085/jgp.201812274>
- [17] Hoffmann, E.K., Lambert, I.H. and Pedersen, S.F. (2009) Physiology of Cell Volume Regulation in Vertebrates. *Physiological Reviews*, **89**, 193-277.
<https://doi.org/10.1152/physrev.00037.2007>
- [18] Ayrapetyan, S.N., Suleymanyan, M.A., Sagian, A.A. and Dadalyan, S.S. (1984) Au-

- toregulation of Electrogenic Sodium Pump. *Cellular and Molecular Neurobiology*, **4**, 367-384. <https://doi.org/10.1007/BF00733598>
- [19] Carpenter, D.O., Fejtl, M., Ayrapetyan, S.N., Szarowski, D.H. and Turner, J.N. (1992) Dynamic Changes in Neuronal Volume Resulting from Osmotic and Sodium Transport Manipulations. *Acta Biologica Hungarica*, **43**, 39-48.
- [20] Palade, G.E. (1953) Fine Structure of Blood Capillaries. *Journal of Applied Physics*, **24**, 1424-1432.
- [21] Parton, R.G. and Simons, K. (2007) The Multiple Faces of Caveolae. *Nature Reviews*, **8**, 185-194. <https://doi.org/10.1038/nrm2122>
- [22] Cooke, K.R. (1981) Ouabain and Regulation of Cellular Volume in Slices of Mammalian Renal Cortex. *The Journal of Physiology*, **320**, 319-332. <https://doi.org/10.1113/jphysiol.1981.sp013952>
- [23] Cooke, K.R. (1978) Ouabain and Regulation of Cellular Volume in Freshly Prepared Slices of Rabbit Renal Cortex. *The Journal of Physiology*, **279**, 361-374. <https://doi.org/10.1113/jphysiol.1978.sp012349>
- [24] Ayrapetyan, S.N. and Suleymanian, M.A. (1979) On the Pump-Induced Cell Volume Changes. *Comparative Biochemistry and Physiology*, **64A**, 571-575. [https://doi.org/10.1016/0300-9629\(79\)90585-1](https://doi.org/10.1016/0300-9629(79)90585-1)
- [25] Bloedel, J., Gage, P.W., Llinás, R. and Quastel, D.M. (1966) Transmitter Release at the Squid Giant Synapse in the Presence of Tetrodotoxin. *Nature*, **212**, 49-50. <https://doi.org/10.1038/212049a0>
- [26] Iwasa, K., Tasaki, I. and Gibbons, R.C. (1980) Swelling of Nerve Fibers Associated with Action Potentials. *Science*, **210**, 338-339. <https://doi.org/10.1126/science.7423196>
- [27] Terakawa, S. (1990) Intracellular Pressure and the Excitable Membrane. In: Ayrapetyan, S.N., Ed., *Metabolic Regulation of Membrane Function*, Academy of Sciences of Armenian SSR Publishing, Yerevan, 140-148.
- [28] Kojima, M., Ayrapetyan, S. and Koketsu K. (1984) On the Membrane Potential Independent Mechanism of Sodium Pump-Induced Inhibition of Spontaneous Electrical Activity of Japanese Land Snail Neurons. *Comparative Biochemistry and Physiology*, **77**, 577-583. [https://doi.org/10.1016/0300-9629\(84\)90232-9](https://doi.org/10.1016/0300-9629(84)90232-9)
- [29] Ayrapetyan, S.N., Rychkov, G.Y. and Suleymanian, M.A. (1988) Effects of Water Flow on Transmembrane Ionic Currents in Neurons of Helix Pomatia and in Squid Giant Axon. *Comparative Biochemistry and Physiology*, **89**, 179-186. [https://doi.org/10.1016/0300-9629\(88\)91076-6](https://doi.org/10.1016/0300-9629(88)91076-6)
- [30] Rychkov, G.Y., Suleymanian, M.A. and Ayrapetyan, S.N. (1989) The Dependence of Water Flow Effect on the Ionic Currents of Dialyzed Neuron on Fluidity of Somatic Membrane. *Biological Membranes*, **6**, 733-740. (In Russian)
- [31] Suleymanian, M.A., Ayrapetyan, S.N., Arakelyan, V.B. and Ayrapetyan, V.Y. (1993) The Effect of Osmotic Gradient on the Outward Potassium Current in Dialyzed Neurons of Helix Pomatia. *Cellular and Molecular Neurobiology*, **13**, 183-190. <https://doi.org/10.1007/BF00735374>
- [32] Baker, P.F., Hodgkin, A.L. and Shaw, T.I. (1962) The Effects of Changes in Internal Ionic Concentrations on the Electrical Properties of Perfused Giant Axons. *The Journal of Physiology*, **164**, 355-374. <https://doi.org/10.1113/jphysiol.1962.sp007026>
- [33] Ayrapetyan, S.N. (1985) Activation and Inactivation Effect of the Transmembrane Water Flows on the Transmembrane Currents in Squid Giant Axon. *Biological Journal of Armenia*, **38**, 245-250.

- [34] Keynes, R.D. (1965) Energy Transformations in the Generation of Bioelectricity. In: Chance, B., Estabrook, R.W. and Williamson, J.R., Eds., *Control of Energy Metabolism*, Academic Press, New York, 375-381.
<https://doi.org/10.1016/B978-1-4832-3161-7.50046-X>
- [35] Mullins, L.J. and Awad, M.Z. (1965) The Control of the Membrane Potential of Muscle Fibers by the Sodium Pump. *Journal of General Physiology*, **48**, 761-775.
<https://doi.org/10.1085/jgp.48.5.761>
- [36] Venosa, R.A. (1978) Stimulation of the Na⁺-Pump by Hypotonic Solutions in Skeletal Muscle. *Biochimica et Biophysica Acta*, **510**, 378-383.
[https://doi.org/10.1016/0005-2736\(78\)90038-X](https://doi.org/10.1016/0005-2736(78)90038-X)
- [37] Ayrapetyan, S.N. (1976) Involvement of the Na Pump in Slow Oscillations Underlying the Bursting Patterns in Helix Neurons. In: Salanki, J., Ed., *Neurobiology of Invertebrates*, Academiai Kiado, Budapest, 353-370.
- [38] Ayrapetyan, S.N., Arvanov, V.L., Maginyan, S.B. and Azatyan, K.V. (1985) Further Study of the Correlation between Na-pump Activity and Membrane Chemosensitivity. *Cellular and Molecular Neurobiology*, **5**, 231-243.
<https://doi.org/10.1007/BF00711009>
- [39] Pivavarov, A.S., Calahorro, F. and Walker, R.J. (2019) Na/K Pump and Neurotransmitters Membrane Receptor. *Invertebrate Neuroscience*, **19**, 1-27.
<https://doi.org/10.1007/s10158-018-0221-7>
- [40] Baker, P.F., Blaustein, M.P., Hodgkin, A.L. and Steinhardt, S.A. (1969) The Influence of Ca on Na Efflux in Squid Axons. *The Journal of Physiology*, **200**, 431-458.
<https://doi.org/10.1113/jphysiol.1969.sp008702>
- [41] Juhaszova, M. and Blaustein, M. (1982) Na⁺ Pump Low and High Ouabain Affinity Alpha Subunit Isoforms Are Differently Distributed in Cells. *Proceedings of The National Academy of Sciences of the United States of America*, **94**, 1800-1805.
<https://doi.org/10.1073/pnas.94.5.1800>
- [42] Blaustein, M.P. and Lederer, W.J. (1999) Na/Ca Exchange. Its Physiological Implications. *Physiological Reviews*, **79**, 763-854.
<https://doi.org/10.1152/physrev.1999.79.3.763>
- [43] Sagian, A.A., Ayrapetyan, S.N. and Carpenter, D.O. (1996) Low Dose of Ouabain Stimulates the Na:Ca Exchange in Helix Neurons. *Cellular and Molecular Neurobiology*, **16**, 180-192. <https://doi.org/10.1007/BF02150229>
- [44] Ayrapetyan, S. (2012) Cell Hydration as a Universal Marker for Detection of Environmental Pollution. *Environmentalist*, **32**, 210-221.
<https://doi.org/10.1007/s10669-011-9380-3>
- [45] Dadalyan, S.S., Kiss, T., Azatyan, K.V., Ayrapetyan, S.N. and Salanki, J. (1988) The Effect of Low Concentration of GABA on the ACH Sensitivity of Snail Neurons. In: Salanki, J., Ed., *Neurobiology of Invertebrates*, Academiai Kiado, Budapest, 643-653.
- [46] Ayrapetyan, S. and Carpenter, D.O. (1991) On the Modulatory Role of Extra-Low Concentrations of Synaptic Transmitters for Membrane Functional Activity. *Journal of Evolutionary Biochemistry and Physiology*, **26**, 513-528.
- [47] Ayrapetyan, S.N. (2006) Cell Aqua Medium as a Preliminary Target for the Effect of Electromagnetic Fields. In: Ayrapetyan, S.N. and Markov, M.S., Eds., *Bioelectromagnetics. Current Concepts. NATO Security through Science Series*, Springer Press, Netherlands, 31-64. https://doi.org/10.1007/1-4020-4278-7_3
- [48] Ayrapetyan, S.N. (2015) The Role of Cell Hydration in Realization of Biological Effects of Non-Ionizing Radiation (NIR). *Electromagnetic Biology and Medicine*, **34**,

- 197-210. <https://doi.org/10.3109/15368378.2015.1076443>
- [49] Clark, R.B. (2013) Profile of Kobilka BK, Lefkowitz RJ. Nobel Laureates in Chemistry. *Proceedings of The National Academy of Sciences of The United States of America*, **110**, 5274-5275. <https://doi.org/10.1073/pnas.1221820110>
- [50] Xie, Z. and Askari, A. (2002) Na/K ATPase as a Signal Transducer. *European Journal of Biochemistry*, **269**, 2434-2439. <https://doi.org/10.1046/j.1432-1033.2002.02910.x>
- [51] Askari, A. (2019) The Sodium Pump and Digitalis Drugs: Dogmas and Fallacies. *Pharmacology Research & Perspectives*, **2019**, e00505. <https://doi.org/10.1002/prp2.505>
- [52] Ayrapetyan, S.N., Avanesian, A.S., Avetisian TH and Majinian, S.B. (2017) Physiological Effects of Magnetic Fields May Be Mediated through Actions on the State of Calcium Ions in Solution. In: Carpenter, D. and Ayrapetyan, S., Eds., *Biological Effects of Electric and Magnetic Fields*, Volume 1, Academic Press, New York, 181-192. <https://doi.org/10.1016/B978-0-12-160261-1.50012-2>
- [53] Ayrapetyan, S. (2013) Na⁺/K⁺ Pump $\alpha 3$ Isoform is a Universal Membrane Sensor for Weak Environmental Signals. *Journal of Bioequivalence & Bioavailability*, **5**, 31-40. <https://doi.org/10.4172/jbb.1000131>
- [54] Brini, M. and Carifolly, E. (2009) Calcium Pumps in Health and Disease. *Physiological Reviews*, **9**, 1341-1378. <https://doi.org/10.1152/physrev.00032.2008>
- [55] Ayrapetyan, S. (2001) Na-K Pump and Na:Ca Exchanger as Metabolic Regulators and Sensors for Extra-Weak Signals in Neuromembrane. In: Ayrapetyan, S.N. and North, A.C.T., Eds., *Modern Problems of Cellular and Molecular Biophysics*, Noyantapan, Yerevan, 31-57.
- [56] Azatian, K.V., Karapetian, I.C. and Ayrapetyan, S.N. (1993) Effect of Low Dose Acetylcholine on Ca Ions Influx into Helix Pomatia Neurons. *Biological Membranes*, **10**, 317-320.
- [57] Azatian, K.V., Ayrapetyan, S.N. and Carpenter, D.O. (1997) Metabotropic GABA Receptors Regulate Acetylcholine Responses on Snail Neurons. *General Pharmacology*, **29**, 67-72. [https://doi.org/10.1016/S0306-3623\(96\)00568-X](https://doi.org/10.1016/S0306-3623(96)00568-X)
- [58] Saghian, A.A., Dadalian, S.S., Takenaka, T., Suleymanian, M. and Ayrapetyan, S.N. (1986) The Effect of Short-Chain Fatty Acids on the Neuronal Membrane Function. 3. The Na Efflux from the Cells. *Cellular and Molecular Neurobiology*, **6**, 397-405. <https://doi.org/10.1007/BF00711408>
- [59] Arvanov, V.L., Takenaka, T., Dadalian, S.S. and Ayrapetyan, S.N. (1986) The Effect of Short-Chain Fatty Acids on the Neuronal Membrane Functions of Helix fPomatia. 2. Cholinergic Properties. *Cellular and Molecular Neurobiology*, **6**, 165-175. <https://doi.org/10.1007/BF00711068>
- [60] Suleymanian, M., Takenaka, T., Stamboltsyan, K. and Ayrapetyan, S. (1986) The Effect of Short-Chain Fatty Acids on the Neuronal Membrane Functions of Helix Pomatia. *Cellular and Molecular Neurobiology*, **6**, 151-163. <https://doi.org/10.1007/BF00711067>
- [61] Ayrapetyan, S., Yeganyan, L., Bazikyan, G., Muradyan, R. and Arsenyan, F. (2012) Na⁺/K⁺ Pump $\alpha 3$ Isoform-Dependent Cell Hydration Controlling Signaling System Dysfunction as a Primary Mechanism for Carcinogenesis. *Journal of Bioequivalence & Bioavailability*, **4**, 112-120. <https://doi.org/10.4172/jbb.1000123>
- [62] Dvoretzky, A.I., Ayrapetyan, S.N. and Shainskaya, A.M. (2012) High-Affinity Ouabain Receptors: Primary Membrane Sensors for Ionizing Radiation. *The Environ-*

- mentalist*, **32**, 242-248. <https://doi.org/10.1007/s10669-012-9393-6>
- [63] Mikaelyan, Y. and Ayrapetyan, S. (2019) Over-Expression of Na/Ca Exchangers in Soft Tissues as a Novel Diagnostic Marker for Carcinogenesis. *Cancer Research and Molecular Mechanisms*, **5**.
- [64] Mikaelyan, Y., Eloyan, N. and Ayrapetyan, S. (2019) The Na/Ca Exchange as a Target for Antitumor Effect of 4Hz Pulsing Magnetic Field. *Electromagnetic Biology and Medicine*, **219**, 1-9. <https://doi.org/10.1080/15368378.2019.1685542>
- [65] Narinyan, L. and Ayrapetyan S. (2019) Age-Dependent Comparative Study of 4Hz and 8Hz EMF Exposure on Heart Muscle Tissue Hydration of Rats. *Open Journal of Biophysics*, **9**, 70-82. <https://doi.org/10.4236/ojbiphy.2019.91005>
- [66] Narinyan, L., Ayrapetyan, G. and Ayrapetyan, S. (2013) Age-Dependent Magneto-sensitivity of Heart Muscle Ouabain Receptors. *Bioelectromagnetics*, **34**, 312-322. <https://doi.org/10.1002/bem.21769>
- [67] Narinyan, L. and Ayrapetyan, S. (2019) Age-Dependent Impairment of Heart Muscle Contractility as a Primary Mechanism for Overexpression of Na/Ca Exchanger in Brain Cortex Tissues. *European Journal of Biophysics*, **7**, 27-42.
- [68] Nikoghosyan, A., Heqimyan, A. and Ayrapetyan, S. (2019) Aging Leads to Over-Expression of Na⁺/K⁺ Pump Units in Liver and Na⁺/Ca²⁺ Exchangers in Brain Cortex. *Open Journal of Biophysics*, **9**, 218-237. <https://doi.org/10.4236/ojbiphy.2019.93016>

A Short Note on Containment Scheme against Spreading of Novel Coronavirus COVID-19

Wan Ki Chow¹, Cheuk Lun Chow²

¹Department of Building Services Engineering, The Hong Kong Polytechnic University, Hong Kong, China

²Department of Architecture and Civil Engineering, City University of Hong Kong, Hong Kong, China

Email: wan-ki.chow@polyu.edu.hk

How to cite this paper: Chow, W.K. and Chow, C.L. (2020) A Short Note on Containment Scheme against Spreading of Novel Coronavirus COVID-19. *Open Journal of Biophysics*, 10, 84-87.

<https://doi.org/10.4236/ojbiphy.2020.102007>

Received: March 11, 2020

Accepted: March 27, 2020

Published: March 30, 2020

Copyright © 2020 by author(s) and Scientific Research Publishing Inc.

This work is licensed under the Creative Commons Attribution International License (CC BY 4.0).

<http://creativecommons.org/licenses/by/4.0/>



Open Access

Abstract

A two-stage containment scheme is proposed to minimize spreading of the novel coronavirus. Two stages of quarantine each of 14 days will be involved.

Keywords

Coronavirus, Containment Scheme, Safety Management, Quarantine Control

1. Introduction

Spreading of the novel coronavirus (COVID-19) [1] among people is fast. As this is a novel coronavirus disease, some of its characteristics are unlike the previous coronaviruses, and still unknown. These novel characteristics make spreading control [2] [3] [4] scheme difficult. The physics behind was just proposed [5] recently. Two points are of particular importance in this respect. The first point is that the incubation period, which is commonly taken to be 14 days (based on SARS), may be longer than this and an incubation period of up to 24 days has been reported. The second point is asymptomatic subjects, that is, people still in the incubation period, are contagious. Based on these two points the present 14-day quarantine practice might not be adequate.

It appears that this epidemic will not come to an end in a short time [6], and might last till the end of the year 2020. A better way at this stage (March of 2020) is to block or minimize contact among people within a reasonable time, as proposed below, which is a compromise between effectiveness (requiring longer quarantine) and degree of freedom (less restriction on people quarantined).

Symptoms of COVID-19 can be observed only after the incubation period, commonly taken to be 14 days [1]. Therefore, a viable containment strategy of quarantine of suspected subjects to prevent further disease spreading is needed.

It is very difficult to realize complete isolation of suspected subjects if there are no serious consequences. Too many people might have been infected already if the quarantine requirement is too loose or the quarantine period is too short.

A safety management scheme arranging quarantine is therefore proposed in this short note based on the following containment scheme which is to be imposed on asymptomatic people identified to have been in close contact with confirmed subjects or have a travel history in certain areas (as specified by the government).

2. First Stage Quarantine

The containment scheme is as follows:

F1. Divide the containment area to be controlled into n blocks, $N_1, N_2, \dots, N_i, \dots, N_n$, where the i^{th} block N_i can be a city, a town, a village, a housing estate, a building or even a cruise ship [7] ... etc.

F2. Divide the i^{th} block N_i into m units, $M_{i1}, M_{i2}, \dots, M_{ij}, \dots, M_{im}$, where the j^{th} unit M_{ij} of the i^{th} block N_i can be a home, a level in a building, several buildings or even a residential area as in **Figure 1**.

F3. The smaller the size of the j^{th} unit M_{ij} of the i^{th} block, the more effective will be the control of spreading.

F4. Contact is only allowed within the unit M_{ij} , but prohibited among the other units of the block N_i in 14 days.

F5. Identify infected patients for medical treatment. If there is a confirmed case in unit M_{ij} during this stage, quarantine of the people in that unit will continue for 14 days starting from the date of confirmation of their unit-mate.

3. Second Stage Quarantine

People passing the first stage of quarantine will proceed to the second stage of quarantine, which is a relaxation of the first stage. This stage is designed based on compromise between safety and degree of freedom.

S1. Contact among different units M_{ij} inside the i^{th} containment block N_i is allowed in this stage, but not among different containment blocks in another 14 days.

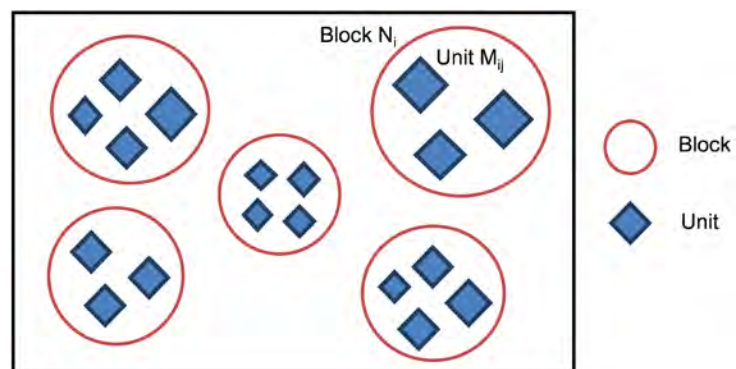


Figure 1. Blocks and units.

S2. Identify the infected patients in each containment block for medical treatment. If there is a confirmed case in the i^{th} block N_i during this stage, quarantine of the people in that block will continue for 14 days starting from the date of confirmation of their block-mate.

4. Releasing Stage

People passing these two stages of quarantine will be released if laboratory check for the novel coronavirus cannot be arranged due to resources limitation.

5. Conclusions

The following can be concluded:

- The above recommended containment scheme requires 2 quarantine levels of 14 days each (totally 28 days) to minimize the spreading of COVID-19.
- The scheme is a compromise between effectiveness and degree of freedom.

Conflicts of Interest

The authors declare no conflicts of interest regarding the publication of this paper.

References

- [1] Edwards, E. (2020) Coronavirus Gets Official Name from WHO: COVID-19. NBC News, 12 February 2020. <https://www.nbcnews.com/health/health-news/coronavirus-gets-official-name-who-covid-19-n1134756>
- [2] Chinese Association of Refrigeration (2020) Some Explanations and Suggestions on the 'Aerosol Transmission' of COVID-19 in Recent Days. 2 February 2020. (In Chinese) http://www.car.org.cn/index.php?s=/articles_1349.html
- [3] Life Times (2020) What Is the Probability of Virus Spreading on the Plane? A Diagrammatic Sketch to Show You Clearly. 3 February 2020. (In Chinese) https://mp.weixin.qq.com/s?__biz=MjM5OTgyODIwMQ==&mid=2653043885&idx=1&sn=1376c5ff8bac53b26b2719538768bfb&key=42cbd266dd78a82132d020bdb75eaf2094e688076b2027a12d2b3a7df3e66380e99e9812c6757d427f66eee9f9758419d4c4f87cf44c688988fd28dfb5cf8bc79f1a14b68eb3a83517fbaddec4098c2e&scene=1&uin=MjY2MzEyNzE1&devicetype=Windows+7&version=62080079&lang=zh_CN&exportkey=AVS%2BVR%2BE92Pc4hO%2Fn31oae0%3D&pass_ticket=%2FowRwMK9LKpR699C5hwy06zAwqGb8lzTsVzfltNusI0%3D
- [4] Gale, J. (2020) Prognosis: There Is a 'Tipping Point' before Coronavirus Kills. Bloomberg. <https://apple.news/A4yrwqSUyRT2tL4oh4tsVHw>
- [5] Wong, K.W., Fung, P.C.W. and Chow, W.K. (2020) Solar Radiation, Perelman Entropy Mapping, DNA, Viruses Etc. *Open Journal of Biophysics*, **10**, 54-58.
- [6] RTHK English News (2020) Covid-19 Here to Stay, Says Top Microbiologist. 8 March 2020. <https://gbcode.rthk.hk/TuniS/news.rthk.hk/rthk/en/component/k2/1513140-20200308.htm>
- [7] The Guardian (2020) Coronavirus: Woman on Diamond Princess Cruise Ship Tested Positive after Disembarking.

<https://www.theguardian.com/world/2020/feb/23/coronavirus-woman-on-diamond-princess-cruise-ship-tested-positive-after-disembarking>

Nomenclature

M—the unit within a block

N—the block

Subscripts

i—number of the block

j—number of the unit in a block

COVID-19: A Physical Model

Kai W. Wong¹, Peter C. W. Fung², Wan K. Chow³

¹Department of Physics and Astronomy, University of Kansas, Lawrence, USA

²Department of Physics, Department of Medicine, and Centre on Behavioral Health, University of Hong Kong, Hong Kong, China

³Department of Building Services Engineering, The Hong Kong Polytechnic University, Hong Kong, China

Email: kww88ng@gmail.com

How to cite this paper: Wong, K.W., Fung, P.C.W. and Chow, W.K. (2020) COVID-19: A Physical Model. *Open Journal of Biophysics*, 10, 88-95.
<https://doi.org/10.4236/ojbiphy.2020.102008>

Received: March 21, 2020

Accepted: April 11, 2020

Published: April 14, 2020

Copyright © 2020 by author(s) and
Scientific Research Publishing Inc.

This work is licensed under the Creative
Commons Attribution International
License (CC BY 4.0).

<http://creativecommons.org/licenses/by/4.0/>



Open Access

Abstract

The coronavirus structure is explained as a fractal representation of the Poincare sphere of proteins, dotted with t-spikes having the geometric realization of the SU(3) Lie group for the protein spike, and encompasses an RNA of SU(2) topologies representations, while within the core contains a virus DNA. Through this suggested model, the virus must possess a critical temperature T_c , induced by the EEM mechanism for the completion of the Poincare sphere surface. Thus above T_c it will disintegrate. We then discuss how the virus transmission progresses within the patient's body, and explain a very fast recent detection method currently used consistent with this model, as well as a corresponding possible cure based on this same principle of the body's immune system. Hopefully the model can be also used as a guide to finding possible medications, so far is lacking.

Keywords

COVID-19, Perelman Mappings, Virus Survival Temperature T_c ,
Virus Multiplication Mechanism

1. Introduction and the Physical Model

The recent coronavirus pandemic has created great economic damages to the world on top of the health pandemic. On the other side, because of this disaster we have learned a lot about the structure and progress and multiplication mechanisms of the virus in the human body. We shall try to explain below how we can apply physical principles derived from Perelman mappings of the homogeneous 5D space-time into its physical shape and summarize this deadly COVID-19 operation.

All coronaviruses are basically spherical in shape, covered with “t” shape spikes on the surface. Each virus spike contains a unique RNA within. And each

spike is a protein composed of 3 vertical parallel strains, displaying the SU(3) fractal representation of the proton/neutron formation from the quark model, and enclosing a linear void in the center, clearly showing the potential of housing an RNA structure. The spherical surface is a lipid bilayer on which many proteins are inserted. Some of these proteins have very strong “intruding power” so that the virus lets itself be engulfed by many types of living cells when in contact. The virus attacks not only respiratory cells, but can get into gastric cells, or even neurons. It cannot enter the skin which is protected by the epithelium. In terms of 5D projection into the Lorentz 4D manifold physical principles, it implies the virus is formed through the two steps of Perelman mappings, such that its topological surface must repeat the SU(3) and SU(2) Lie group symmetry [1], by gathering the proteins within the surrounding thermal bath, as induced by the DNA spectrum, which is the eigen-solutions of the Maxwell DLRO (Diagonal Long Range Order) monopole loop created via thermal energy supplied to the DNA, as explained by us earlier [2], while according to the Excitonic Enhancement mechanism model [3], the formation of the spherical protein coating requires the temperature below a control value T_c of the ODLRO (Off-diagonal Long Range Order) on the Valence band “p” electron hole orbitals [4]. Hence, we expect the surface to be dotted with t-spikes, having structure of 3 gathered in the corners of an equilateral triangle, representing SU(3) topology, while a 1-dimensional monopole $2ec$ expanding boson field composed of $e, -e$ massless spinor pair if allowed, would be along the RNA, except due to the finite fixed length of the RNA it does not exist as explained in ref. [2] through the center of the triangle, thus obeying SU(2). (See **Figure 1** for illustration of the virus.)

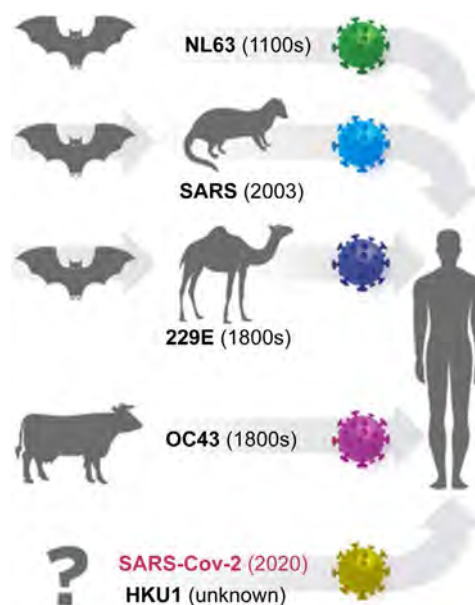


Figure 1. Epidemic potential. (Source: Timothy Sheahan, University of North Carolina. In: B. McKay and T. Ansari, “Coronavirus Symptoms and How to Protect Yourself: What We Know”, The Wall Street Journal, 19 March 2020.

<https://www.wsj.com/articles/what-we-know-about-the-coronavirus-11579716128>)

Because such a structure is the simplest fractal topological structure that we can create out of Perelman mappings into a Poincare sphere due to the necessary realization in the 4D Lorentz space-time from the homogeneous 5D mapping. The varying sizes and varying number of spikes make the different Coronaviruses. The monopole eigen-state within the DNA energy must be maintained via chemical decomposition of matters in the surrounding via oxidation or external optical source, such as thermal or light sources. Without the energy, the monopole will decay, and the virus will also decompose, releasing the RNAs in the “t” spikes. For each pair of such RNAs, when energy is available, the nitrogenous end caps Uracil will be replaced by the Thymine in the DNA. To achieve this, the loss spikes must be attached first to the patient’s oxidation energy source, so that the released RNA can form new DNA. Then through the Perelman 3D entropy manifold mapping the new virus can be created. This is the main reason why the coronavirus must attach itself to the respiratory path wall. Furthermore, as that happens that when a new virus can be born, the temperature in the surrounding must increase, but it must remain not to exceed T_c for the shell formation: This is a very delicate constrain.

To understand quantitatively, let us review the Excitonic Enhancement Mechanism model [3] that was proposed for the HTC High Temperature Cuprates Superconductors [5], where the ODLRO of the VB valence bond ‘p’ holes orbitals were induced via the formation of excitons between the Fermi level and the CB conduction band and its coupling to the holes in place of the phonons in the BCS superconductor mechanism. By extending this model for the natural formation of bio cells within the human body, we can provide an estimation on the T_c in normal human cells.

According to the 5D model, the cell growth is caused by the induced ODLRO in the VB “p” hole orbitals, which comes from the periodic Oxygen in the CuO plane for the cuprate superconductors, and the Carbon in the periodic spherical surface protein shell for the bio cells, and similarly the coronavirus, via the EEM mechanism.

The normal body temperature is roughly 100°F, or 36°C, which corresponds to 309°K. In order for the normal growth T_c must be > than this temperature. Let us assume then $T_c = 311^\circ\text{K}$.

The EEM superconducting gap Δ_G [6] is given by

$$\Delta_G = \left\{ \Delta_{BCS}^2 + \Delta_{ex}^4 / [e_o + \mu + G]^2 \right\}^{0.5} \quad (1)$$

[see Wong and Ching papers on the derivation of Equation (1) in the EEM theory]

Δ_{ex} is the exciton binding, and $\langle \mu + G$, G is the positive bandgap, while μ is the Fermi level of the holes. ε_o is the correction due to the presence of excitons.

Using the Boltzmann constant $k_B = 1.38 \times 10^{-23} \text{ J/K}$.

By ignoring Δ_{BCS} and ε_o , we obtain a numerical result

$$\mu + G \text{ of } 2 \text{ eV} \quad (2)$$

and Δ_{ex} of 1 eV. that would satisfy a T_c of 311°K.

For HTS cuprates Δ_{ex} is roughly 0.5 - 0.6 eV, while the rest of the electron band structure parameters μ and G are similar. We then expect T_c to be no more than 120°K. The enhanced T_c in bio cells must be much higher, in fact higher than the body normal temperature, due essentially to the exciton effective mass being smaller.

This quantitative analysis is equally applicable for estimating the Coronaviruses T_c . In fact it must lie above the body cells T_c , but less than the max fever T before the onset of pneumonia, which can be set as 20°K higher. Hence the T_c for the Coronaviruses which covers from the common flu to SARS and MERS, must be between 311°K to 331°K.

As the body T raises close to T_c of the virus, the virus multiplication slows, due primarily to the EEM induced broadening of the HTC transition. Thus the most active T range of the virus must be between the body's normal T and its T_c value. Suppose the COVID-19 $T_c = 330^\circ\text{K}$, and is most active around the body T , since the reproduction probability follows an exponential curve, which governs the rate of transmission within a human population. This works out to 36°C. As temperature raises above 36°C, the virus reproduction decreases rapidly.

The higher the shell formation T_c , the more deadly it would be, because it can multiply easier. However it also implies the monopole eigen-energy requirement is also higher, which in turn due to the uncertainty principle $dE \cdot dt \geq \hbar$, tends to shorten the life time of the virus which is proportional to dt , thus reduces its effective ability to transmit when away from the human body. As such, due to the environment content of proteins available, and the T value reachable, the virus for its own survival constantly makes minor changes, very much like the common flu viruses.

As shown in **Figure 1**, most Coronaviruses are carried by bats, where the viruses must be harmless, means the bats body immune and protein composition does not favor the multiplication of the virus. This same principle probably explains why COVID-19 is less deadly in kids than adults. A better quantitative research on the general protein compositional changes with our body aging could be helpful in our search of a prevention.

2. Mechanism of Propagation of COVID-19 within the Patient

It is due to the above explanation, the first stage symptom of the COVID-19 in a patient is always fever [7] as new viruses are formed from the spikes penetrating into a body's cell so that the RNA length can be extended temporarily to accommodate the creation of a 2ec monopole boson, accompanied with the oxidation of the proteins on the virus shell, which in turn breaks the virus shell so as to be able to change the RNA end caps from Uracil to the Thymine and created the DNA, from which new coronavirus can be formed around it as we discussed in the previous section. Hence it is most efficient for the virus to multiply along the respiratory track. This T raises coincide with inducing the body's immune

response, which operates as T rises, and in turn triggers the white blood T cells to seek and consume the virus. Thus young healthy people usually can recover as the white blood T cells win over the limited number of new rebirth of the viruses, due primarily from limited proteins available caused by the lack of extra sugars and fat proteins generally present in older people. At this stage, when many new viruses are created from the dead ones left over for a patient in the respiratory track are sometimes accompanied with dry cough as the body's respiratory expels the dead virus that did not make it revived by forming new viruses. With that life viruses are also ejected, thus spreading the virus transmission in droplets covering the near surrounding. Hence to slow down the direct person to person transmission of the virus, social distancing, frequent sensitizing including hands, patient isolation, and population mobility confinement is of paramount importance. Disposed dead virus must remain within the patient's blood for some time, as the immune mechanism that destroys the virus is through the T-cells, which of course is carried through the body by the blood flow. Hence, it is easy to detect the Coronavirus infected patient via blood test for the presence of the virus DNA, even when the patient had totally recovered. This technique of testing has in fact been created and applied by the company Biomerica, as a demonstration of its erology patented method. The test is simple and the result is 100% and very quick, except it gives false positive if the patient already recovered. Hence the positive test must be simultaneously verified by direct detection of the virus present in the mucus obtained from the throat, plus no lung cell damage using X-ray photographs or CT scan. The coronavirus detection must then always be simultaneously cross verified with all three detection methods. When the immune response fails for the first stage, the virus will find its path to enter the lung. At this final stage, the virus is attached to the lung cells. The death of a virus, will produce mucus which is the waste left from the protein broken shell, which in turn clog up the effective average air cell volume, thus changing through the general gas law: $PV/T = \text{constant}$, where P is the air pressure within the lung cells, V is the effective lung cell column. Thus the reduction of V lowers the T in the lung. A severe T drop below T_c leads to even more virus creation ending in Pneumonia for the patient, and high fever returns again, even with $T > T_c$. But before that, the patient can lose the battle for life, before the virus is destroyed by the breaking of the ODLRO transition as the fever's T exceeds T_c , causing the virus self-reduction. Hence, at this last stage, buying time is essential. The only method then is to keep the effective air and oxygen volume in the lung as long as possible. Unfortunately, even if the patient recovers from this stage, his or her lung cells might be permanently compromised, leaving a lifelong damage.

3. Conclusion and Some Suggestions for the COVID-19 Medication

We look at the HTC crystals. That is formed by simple phase transition from

liquid to crystal solid, which produces the band structure, with periodic boundary condition. But bio cells do not go through such a phase transition, it is induced by a DLRO within itself. That requires the presence of a DNA, which can have a gene spectrum from the monopole boson DLRO state. Hence the virus must be introduced into a patient from outside. It cannot self-develop within the body. But even with the presence of a virus DNA, that is not enough. The presence of proteins meaning carbon based flexible structures such as ACE2 must be present in virus surrounding thermal bath, then through Perelman entropy mappings it can form the Poincare sphere, which gives the periodic boundary, such that an ODLRO can exist in the electronic orbitals of the shell via EEM to satisfy the LRO matching. This requires also the thermal bath $T < T_c$. Thus DNA must always exist first in every process. Now considering T_c specific to the Coronavirus. To form the DNA, out of just RNAs, is not possible. It needs the original introduction of such a virus DNA into the thermal bath. Then the virus can be generated. In fact, it can multiply, only when RNAs are also present, like human reproduction allowing the genome to track the heritage of the virus [8]. Of all the 9 known Coronaviruses, only 3, that are SARS, MERS and COVID-19 shown to be deadly, the remainders act much like the common flu. Hence we have new DNAs, again all due to DLRO inducing global order. But that needs energy similar to crystal phase transition. Hence there is another $T(o)$ for this to happen. This $T(o)$ needs not to be $<$ or $>$ than T_c for the EEM T_c . The lower $T(o)$ the faster the virus can multiply when one breaks up. The break up comes from multiple possibilities. First, the DNA monopole eigenstate can lose energy to the thermal bath, due to the $h\nu$ spectra, the high ν frequency will lose energy just via conductivity, or T raises to T_c . Hence the virus has to obtain energy input, via extra energy obtained via oxidation in immediate contact. It is this that drives the virus to multiply and survive, and the reason the virus tries to attach itself to the respiratory path, where most oxidation process happens. The more RNAs the spikes carry the faster the virus could evolve, which might make it more or less transmittable, and might end up less deadly to human? Our aim then to eliminate the current COVID-19 pandemic must be a medication that will induce COVID-19 to mutate into a new less deadly form, and to find a vaccine that boosts our immune system to prevent the multiplication of the COVID-19 within our respiratory track.

Because the body's immune response must be accompanied by a temperature rise, it is therefore paramount that COVID-19 patients do not take fever reducing medications.

Through this analysis, we learn not just the progress of COVID-19, but also how simple life cell model like the coronavirus comes about, as well as the triggering of its necessary evolution. The other results we get from this study, allows us to model a prevention of its spread. Obviously, that is naturally accomplished by weather condition changes, through first and foremost the destruction of the monopole spectrum in the DNA, either by lack of energy supply, or by over

supply via climate change. In another word COVID-19, is seasonal, similar to the flu virus. Secondly, as the COVID-19 virus changes, it might either increase or decrease its ability to transmit, as its survival time changes. Thirdly, once the body's immune system recognizes it as an illness, its immune response activation time is shortened by not requiring a raise in body temperature for the white blood T-cell to takeout the virus in the respiratory path. In another word, the body has build-up a natural resistance. Meaning it provides us an immune enhancing mechanism for patients by just having a blood infusion, with the like blood type obtained from COVID-19 100% recovered patients. This process is safe and needs no long time drug testing. But simultaneously it also induces the natural evolution of the virus into another type of Coronavirus, such as SARS. We estimate that the T_c for all coronaviruses lie between 110 - 130°F. With MERS and SARS near the upper limit, COVID-19 is somewhat lower. That means its transmission is reduced in the tropics. Perhaps, we may interpret the current COVID-19 as an evolved form of SARS? And will spread faster. As such, our medication for SARS might be effective also on COVID-19? Furthermore, because for the virus to multiply and survive in the body, its spikes need to be attached to the respiratory path wall, a medication that suppresses that mechanism might also work? That includes medication used for HIV, Malaria and certain antibiotics which raises the virus formation temperature T_c , as some bacterial infection requires that same attachment mechanism to harm the body's cell in the patient. During the early stage of the infection constant drinking of fluid can reduce the virus number along the respiratory upper path by washing the virus into the stomach, where it cannot survive. Therefore, as for medication, we might already have many well-tested drugs such as the Malaria drug helpful to cure COVID-19 for patients in the early stage only. But it is actually dangerous when used in patients already in the last stage, where the virus is destroying the lung. Of course for each of these drugs, testing must be made and effectiveness and side effects verified. As the northern hemisphere starts warming up due to approaching summer, we expect the COVID-19 spread to slow. Unfortunately, it also for the Southern Hemisphere to cool down as there autumn sets in, and we already observe the pandemic centers to shift there. Implying if we do not find a vaccine fast and soon, the pandemic cannot be stopped, and will surely again come back to the northern hemisphere later this year. On the bright side, if we have a vaccine, after this COVID-19 pandemic ends, the human race might for its new generation developed the necessary immune to it, or even new forms of Coronavirus that might come along affecting other mammal species? As to the pandemic's effect on the economy of the world, it will certainly put every country in a sharp depression, at least for 20% decrease in the GDP, or even more. No pandemic in human history has such an economic effect ever happened, even far more severe than the Spanish flu of 1919.

Acknowledgements

We thank Ms. Winnie So for her help in preparing the manuscript.

Conflicts of Interest

The authors declare no conflicts of interest regarding the publication of this paper.

References

- [1] Perelman, G. (2002) The Entropy Formula for the Ricci Flow and Its Geometric Application. arXiv.math.DG/0211159
Perelman, G. (2003) Ricci Flow with Surgery on Three-Manifolds. arXiv.mathDG/0303109
- [2] Wong, K.W., Fung, P.C.W. and Chow, W.K. (2020) Solar Radiation, Perelman Entropy Mapping, DNA, Viruses etc. *Open Journal of Biophysics*, **10**, 54-58. <https://doi.org/10.4236/ojbiphy.2020.102005>
- [3] Ching, W.Y., Xu, Y.N., Zhao, G.L., Wong, K.W. and Zandiehnam, F. (1987) Electronic Structure and Excitonic-Enhanced Superconducting Mechanism in $\text{YBa}_2\text{Cu}_3\text{O}_{7-\delta}$. *Physical Review Letters*, **59**, 1333-1336. <https://doi.org/10.1103/PhysRevLett.59.1333>
- [4] Wong, K.W., Fung, P.C.W. and Chow, W.K. (2019) 5D Model Theory for Creating of Life Forms. *Journal of Modern Physics*, **10**, 1548-1565. <https://doi.org/10.4236/jmp.2019.1013103>
- [5] Wong, K.W. and Ching, C.W. (1988) Thermodynamics of Simultaneous-Excitonic Superconductivity Condensate. *Physica C*, **152**, 397-400. [https://doi.org/10.1016/0921-4534\(88\)90043-3](https://doi.org/10.1016/0921-4534(88)90043-3)
- [6] Wong, K.W. and Ching, C.W. (1989) The Theory of Simultaneous Excitonic-Superconductivity Condensation. *Physica C*, **158**, 1-14. [https://doi.org/10.1016/0921-4534\(89\)90294-3](https://doi.org/10.1016/0921-4534(89)90294-3)
- [7] Maxmen, A. (2020) Slew of Trials Launch to Test Coronavirus Treatments in China. *Nature*, **578**, 347-348. <https://doi.org/10.1038/d41586-020-00444-3>
- [8] Richards, S.E. (2020) How Coronavirus Mutations Can Track Its Spread—And Disprove Conspiracies. *National Geographic*, Coronavirus Coverage.

DNA Sequencing Modified Method through Effective Regulation of Its Translocation Speed in Aqueous Solution

Lusine Gasparyan^{1,2}, Ilya Mazo³, Ferdinand Gasparyan¹, Vahan Simonyan²

¹Yerevan State University, Yerevan, Armenia

²DNA-HIVE LLC, 15313 Diamond Cove Terrace, Rockville, MD, USA

³Argentis LLC, Gaithersburg, MD, USA

Email: fgaspar@ysu.am

How to cite this paper: Gasparyan, L., Mazo, I., Gasparyan, F. and Simonyan, V. (2020) DNA Sequencing Modified Method through Effective Regulation of Its Translocation Speed in Aqueous Solution. *Open Journal of Biophysics*, 10, 96-112.
<https://doi.org/10.4236/ojbiphy.2020.102009>

Received: March 18, 2020

Accepted: April 23, 2020

Published: April 26, 2020

Copyright © 2020 by author(s) and Scientific Research Publishing Inc. This work is licensed under the Creative Commons Attribution International License (CC BY 4.0).

<http://creativecommons.org/licenses/by/4.0/>



Open Access

Abstract

Solid-state nanopore DNA sequencing modified method is developed. Method is based on the tunnel current investigation through the nanopore made on lateral gold electrodes in the form of nanowires or nanoribbons. The movement of DNA in aqueous solution is regulated by the potential applied to reference electrode. The potential applied to the lateral metal electrodes helps to the creation of the molecular junctions. They consist of the nucleosides passing through the pores. Taking into account that DNA moves under gravity, electrophoretic and drag forces, the analytic expression for the DNA translocation speed is calculated and analyzed. The conditions for decreasing the DNA translocation speed or increasing the nucleosides reading time are received. It is shown that one can control value of the DNA molecules bases reading time and the frequency of the bases passes by the choice of magnitude of the potential applied to reference electrode. Our results, therefore potentially suggest a realistic, inherently design-specific, high-throughput nanopore DNA sequencing device/cell as a de-novo alternative to the existing methods.

Keywords

DNA Sequencing, DNA Speed, Forces, Reading Time

1. Introduction

The process of DNA sequencing is a precise determination of the amount and distribution of the nucleotides in DNA molecules. Quick improvements in the cost and speed of DNA sequencing are having a strong influence on comprehen-

sive genome research. Methods of DNA sequencing and their application are detailed analyzed in [1]. In the past decade, the single-nanometer-scale pores demonstrated great capability for the detection, identification, and characterization of DNA [2] [3] and RNA [4] [5]. In recent years, rapid advances have been made and many construction's architectures have been put forward for novel approaches to bio-molecular sensing using nanoelectronics, including the advent of tunnel junctions as a sensing platform. Within the past decade, nanogap electrodes have attracted a lot of attention because of their potential applications in the progressive miniaturization of electronics and as nanoscale tool for analysis of single molecular properties. DNA bases can be identified statistically in nanopore translocation events. Nanogap electrodes can be simply defined as a pair of electrodes with a gap that can be measured in nanometers. The transport dynamics of the charged molecules in the nanosize constructions located in aqueous solution environment is the result of multiple factors including, electrostatic and hydrodynamic interactions, drift and diffusion.

One major challenge of nanopore-based DNA sequencing technology is to find an efficient way to reduce DNA translocation speed. It is necessary that each nucleotide can reside long enough in the measuring pore for creation molecular junctions. Magnitudes of those current will help identification of nucleotides [6]. In order to take control of the DNA molecule translation process, various theories and approaches have been put forward in recent decades.

Authors of Ref. [7] considered that the reasonable value of the DNA translocation speed is near to 0.01 - 1 ms per base, which is equivalent to (10 - 1000) bases/s. Peng and Ling reversed the DNA translocation and achieved an average speed of 0.0096 bases/ μ s = 9600 bases/s [8]. As the translocation times depend strongly on the nucleotide type [9], imply that polymer-pore interactions, rather than the more generic hydrodynamic drag, play an important role in determining the translocation dynamics. The interaction of the polymer with pores is described in detail in [9]. In [10], the authors propose a feedback device architecture for regulating DNA translocation by modulating the effective surface charge density of a nanopore wall. It was shown that the rate of DNA movement can be reduced at a rate of about 55 mm/s per 1 mV/nm. The review [11] focuses on a single aspect in the transport dynamics of a polymer drawn inside a nanoscopic channel. Primarily, the dynamics of polynucleotides is discussed. Some of the concepts that are discussed in [11] apply to uncharged polymers.

Thus, a key challenge to DNA sequencing with nanopores is to find methods to slow down and control DNA translocation. DNA translocation speeds can be reduced somewhat by decreasing temperature [12] [13], or increasing solvent viscosity [7] [14], but these methods do not reduce the variations in the translocation dynamics because of DNA-pore interactions [15] [16] [17] [18]. Problems of controlling DNA motion and translocation in a nanopore analyzed also in [19]. The detailed analyses of the literature data, some critical considerations and the potential ways of optimization of DNA nanopore sequencing were presented

in [20]. Some characteristics of ISFET and EIS based DNA sensors are analyzed detailed by us in [21] [22].

In this paper a modified architecture/design for measuring cell of DNA sequencing using tunneling current is offered in order to control and optimize the translocation speed of the DNA molecules. We study the features of the dynamics of the movement of DNA molecule in an aqueous solution under gravity, electrophoretic and drag forces in order to reduce the rate of movement of the DNA and increase DNA reading time.

2. DNA Dynamics and DNA Speed in Aqueous Solution

In **Figure 1** the scheme of architecture/design for investigation of DNA nucleosides sequencing by the solid state nanopore modified method is presented. The electrolytic cell filled by aqueous solution provides with nanopore, reference and back electrodes (RE and BE). The electrical potential applied on the RE/BE promotes directional movement of the charged DNA molecules under the action of an electric field. The potential applied to the lateral metal electrodes M1 and M2 facilitates the creation of molecular junctions with nucleosides. A nanopore consisting of gold electrodes is covered by insulator layer. Contacts to nanopore can be made in the form of nanowires or nano-ribbons (**Figure 1(c)**). Contacts surface area coated by the insulator layer for its protection and for not letting the negatively charged molecules stick the surface of the electrodes. Capture of DNA molecules on the gold electrode surface will create “false” currents and distort the useful signal. If necessary, many nanopores can be mounted in a cell and a multi-nanopore chamber can be created and at the same time many DNA molecules can be studied (**Figure 1(b)**). In **Figure 1(d)** example of molecular junction M1-DNA GC base pair-M2 is presented.

At the bare pore under applied voltage V between metallic electrodes M1 and M2 flow only low ionic current of electrolyte $I_{i\perp}$ in order to pA [6] [23] [24]. Ionic current through the channel sharply decreases (is blockade) while the DNA molecule move under the gravity P , electrophoretic force F_e (migration under applied potential on the reference electrode), drag force F_D and diffusion (connected with ions concentration gradient in solution) become to the pore and blockade the ionic current. When some of nucleotides of DNA [adenine (A), guanine (G), thymine (T), cytosine (C), nucleotide pairs GC, AT, etc.] captured between gold electrodes, they create the electronic bridge and consequently molecular junctions (at the $V \neq 0$, see [6]). So, DNA bases can create individual electronic bridges between gold electrodes and across a pore (through the nucleotide junction) that will flow only tunnel current. Metal electrodes can be made in the form of nanowires/nanoribbons to create, if possible, a large area of coverage of the coming close DNA molecules with several orientations (**Figure 1(c)**). Such a design of the electrodes can be realized using mechanically controllable break-junction (MCBJ) [25] [26] [27], scanning tunnel microscope (STM) [28] or atomic force microscope (AFM) [29] techniques.

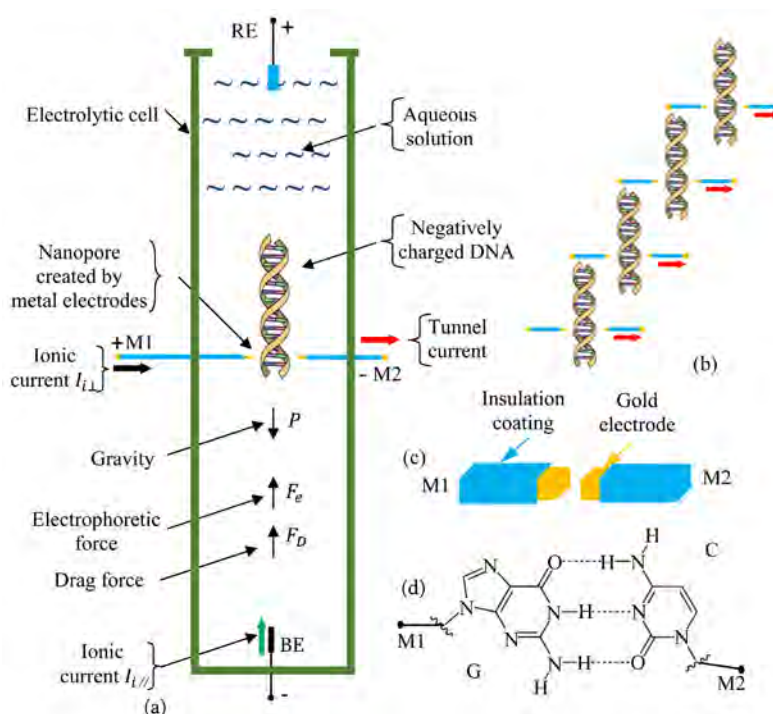


Figure 1. (a) The measurement cell of investigation of DNA nucleosides by the solid state nanopore modified method. (b) Multi-nanopore (4 nanopore) design. (c) Nanopore with nanowire or nanoribbon gold electrodes. (d) Example of molecular junction M1-DNA GC base pair-M2. The potential applied to the electrodes [Au(111)] facilitates the creation of a molecular junction with nucleosides. The Au(111) substrate was chosen as a noble inert substrate to minimize molecule-substrate interactions. Vertical ionic current $I_{i||}$ depend with potential V_0 , applied to RE. Lateral ionic current $I_{i\perp}$ conditioned by potential applied to metallic electrodes. RE means reference electrode, BE means back electrode. It is showing also the gravity (P), electrophoretic (F_e) and drag (F_D) forces, influences on molecules and controlled their movement.

Such a design of electrodes will contribute to almost ~100 percent creation of molecular junctions at any orientation of the DNA. The gap between electrodes must be so narrow that only one DNA molecule passes through it.

For effective reading of nucleotides, it is necessary that they move vertically. The vertically directional movement of the molecule will be determined by the resulting force F

$$F = P + F_e + F_D \quad (1)$$

Let's assume that distribution of the DNA molecules in aqueous solution is homogeneous and DNA concentration gradient in the solution is absence or very small. Then ignoring the role of diffusion and considering that

$$|P| = m_0 g, \quad |F_e| = q \mathcal{E}_0 = \frac{q V_0}{l_0}, \quad |F_D| = \frac{1}{2} \rho v^2 C_D A, \quad (2)$$

for the magnitude of the resulting force we can write:

$$F = m_0 g + |q \mathcal{E}_0| - \frac{1}{2} \rho v^2 C_D A. \quad (3)$$

Here m_0 is the mass of DNA molecule, V_0 is the applied voltage on the reference electrode, l_0 is the distance between RE and nanogap, $\mathcal{E}_0 = V_0/l_0$ is the electric field acting on DNA, $g = 9.80665 \text{ m/s}^2$, q is the negative charge of DNA, v is the speed of the molecule relative to the aqueous solution, A is the molecule cross sectional area, ρ is the density of the solution¹, and C_D is the drag coefficient—a dimensionless number².

Let's discuss the magnitudes of $|\mathbf{P}|$, $|\mathbf{F}_e|$ and $|\mathbf{F}_D|$.

For definiteness assume that DNA consists only from N_n blocks of A, G, C and T nucleotides. Then for m_0 we have:

$$\begin{aligned} m_0 &= N_n (m_A + m_G + m_T + m_C) = \frac{N_n}{N_A} (M_A + M_G + M_T + M_C) \\ &= \frac{N_n}{N_A} \times [M_A (\text{C}_5\text{H}_5\text{N}_5) + M_G (\text{CH}_5\text{N}_5\text{O}) + M_T (\text{C}_5\text{H}_6\text{N}_2\text{O}_2) + M_C (\text{C}_4\text{H}_5\text{N}_3\text{O})] \\ &= \frac{N_n}{N_A} \times [5 \times (12 + 1 + 14) + (12 + 5 \times 1 + 5 \times 14 + 16) \\ &\quad + (5 \times 12 + 6 \times 1 + 2 \times 14 + 2 \times 16) + (4 \times 12 + 5 \times 1 + 3 \times 14 + 16)] \\ &\approx 8 \times 10^{-22} N_n \text{ g} = m_n N_n \text{ kg} \end{aligned}$$

$$m_n = 8 \times 10^{-25} \text{ kg}.$$

Here N_A is the Avogadro number, m_n is the mass of group from four nucleotides, M_A , M_G , M_T and M_C are the molecular masses of adenine ($\text{C}_5\text{H}_5\text{N}_5$), guanine ($\text{CH}_5\text{N}_5\text{O}$), thymine ($\text{C}_5\text{H}_6\text{N}_2\text{O}_2$) and cytosine ($\text{C}_4\text{H}_5\text{N}_3\text{O}$), correspondingly. For example, at the $N_n = 1000$, we have $m_0 \approx 8 \times 10^{-22} \text{ kg}$ and

$$|\mathbf{P}| = 7.84 \times 10^{-21} \text{ N}. \quad (4)$$

The value of F_e depends on \mathcal{E}_0 and for example at the single charged DNA ($q = e = 1.6 \times 10^{-19} \text{ C}$), $V_0 = 2 \text{ V}$ and at the $l_0 = 1 \text{ cm}$ for the $|\mathbf{F}_e|$ we have:

$$|\mathbf{F}_e| = \frac{qV_0}{l_0} = 3.2 \times 10^{-21} \text{ N}. \quad (5)$$

Let's consider the value F_D . Taking $\rho \approx 1 \text{ g/cm}^3 = 10^3 \text{ kg/m}^3$ (as a water, pH = 7), $C_D \approx 0.42$ [9], $A = \frac{\pi d^2}{4} \approx 3.8 \times 10^{-18} \text{ m}^2$ ($d \approx 2.2 \text{ nm}$ is the DNA diameter [31]) we receive

¹Density of the fluid determined by the expression $\rho = 3.446\delta \times 10^{-3} + 1.0048 \text{ g/ml}$ [30], where δ is the percent composition. Density of the fluid changed very little, e.g. at the $0 < \delta \leq 20$, $1 < \rho \leq 1.1 \text{ g/ml}$.

²The drag coefficient C_D depends on the shape of the object and on the Reynolds number $R_e = vD/\nu_0$. Here D is some characteristic diameter or linear dimension and ν_0 is the kinematic viscosity of the fluid. At low R_e C_D is asymptotically proportional to R_e^{-1} , which means that the drag is linearly proportional to the speed. At high R_e C_D is more or less constant and drag will vary as the square of the speed. In the case of high velocity, in general, C_D a function of the orientation of the flow with respect to the molecule (apart from symmetrical objects like a sphere). Assuming that surface area of the DNA molecule end is the half-sphere in further calculations we can take $C_D \approx 0.42$ [9].

$$|F_D| \approx 7.98 \times 10^{-16} v^2 \text{ N}. \quad (6)$$

Where molecule speed v given in m/s.

Now let's determine functional dependency of molecule translocation speed v vs. other parameters, especially vs. V_0 and l_0 . Molecule move under resulting force (3). Kinetic energy of the molecule is equal to work of resulting force. Taking the aqueous solution surface as the origin of coordinate and assume that initial coordinate of molecule is the l_i (Figure 1) and DNA initial speed is v_i we can write

$$\int_{l_i}^{l_0} F dz = \frac{m_0 (v - v_i)^2}{2}$$

Then on the distance $(l_0 - l_i)$ molecule will accumulate the kinetic energy equal to work of resulting force and

$$F(l_0 - l_i) = \frac{m_0 (v - v_i)^2}{2}, \quad (7)$$

or

$$m_0 g + |q\mathcal{E}_0| - \frac{1}{2} \rho v^2 C_D A = \frac{m_0 (v - v_i)^2}{2(l_0 - l_i)},$$

and

$$v - v_i = \left[\frac{2(m_0 g \mp q\mathcal{E}_0)}{m_0 / (l_0 - l_i) + \rho C_D A} \right]^{1/2}. \quad (8)$$

One of significant problems of DNA sequencing is to decrease translocation speed. Assume that molecule starts moving from upper side of chamber ($l_i = 0$) with zero starting speed ($v_i = 0$). For regulating the DNA speed as variable parameters, we can choose l_0 and \mathcal{E}_0 . It is clear also that $v > 0$ and for minimizing v we must put “-” sign in (8) before $q\mathcal{E}_0$ and consider the condition

$$|m_0 g| > |q\mathcal{E}_0| \quad \text{or} \quad \mathcal{E}_0 = \frac{V_0}{l_0} < \frac{m_0 g}{q}. \quad (9)$$

Then expression (8) we can rewrite as

$$v = \left[\frac{2(m_0 g - q\mathcal{E}_0)}{m_0 / l_0 + \rho C_D A} \right]^{1/2}. \quad (10)$$

At the $m_0 \approx 8 \times 10^{-22} \text{ kg}$ ($N_n = 10^3$), $q \equiv e = 1.6 \times 10^{-19} \text{ C}$ and $g \approx 10 \text{ m/s}^2$ the condition (9) equivalent to:

$$\mathcal{E}_0 < 5 \times 10^{-2} \text{ V/m}.$$

Measurements of blockade current of ssDNA in [32] imply that, while polymers longer than the pore they are translocated at a constant speed, the velocity of shorter polymers increases with decreasing length. Note that unlike our case in [32] polarity of the potential applied to gate electrode and electric force directed to opposite (Figure 1(a) in [32]), and velocity quadratically depends on applied field.

As we can see the magnitude of DNA translocation speed strongly depend on \mathcal{E}_0 and the DNA size, particularly on N_n . Using the above parameters, we obtain

$$\frac{m_n N_n}{\rho C_D A l_0} \approx 5 \times 10^{-8} N_n.$$

For the “optimal” case $N_n < 2 \times 10^8$ from (10) we have

$$v \propto \sqrt{N_n}.$$

The schematic behaviors of the molecule speed vs. \mathcal{E}_0 and N_n are shown in **Figure 2**. DNA translocation speed dramatically decreases with the electric field. About such behavior of $v(\mathcal{E}_0)$ is noted also in [10] [11]. Note that the calculated results of [11] predict that for long polymers the translocation mean velocity, defined as the ratio of the polymer contour length and the average first passage time, approaches a constant value that does not depend on N_n . This type of dependence is consistent with our dependencies at the higher values of N_n (saturation of $v(N_n)$) (**Figure 2(b)**).

For receiving low value of speed, we need to minimalized term ($m_0 g - q\mathcal{E}_0$) by the varying \mathcal{E}_0 and N_n . Problem is to find optimal values of \mathcal{E}_0 .

Let's introduce dimensionless electric field strength \mathcal{E} and dimensionless speed v_0 as follows:

$$\mathcal{E} \equiv \frac{q\mathcal{E}_0}{m_0 g}, \quad v_0 \equiv \frac{v}{\sqrt{2gl_0}} \sqrt{1 + \frac{\rho C_D A l_0}{m_0}}. \quad (11)$$

Now expression (10) we can rewrite as follows:

$$v_0 = (1 - \mathcal{E})^{1/2}, \quad \text{or} \quad \lg v_0 = \frac{1}{2} \lg(1 - \mathcal{E}). \quad (12)$$

For receive low speed it is necessary that $(1 - \mathcal{E})$ will be minimal, or with values of \mathcal{E} very close to unity.

Numerical calculations of the DNA translocation speed vs. $(1 - \mathcal{E})$ are carried out. Results of numerical analyzes for DNA three sizes ($N_n = 10^3$, $N_n = 40$ and $N_n = 10$) presented in **Table 1**. Low magnitude of v is obtained with

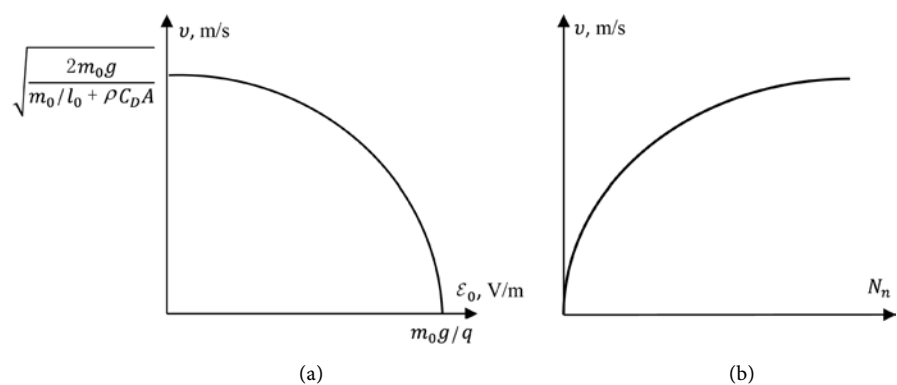


Figure 2. Schematic dependency of the molecule speed vs. \mathcal{E}_0 (a) and N_n (b).

Table 1. Numerical data of the DNA translocation speed for cases $N_n = 1000, 40$ and 10 .

$N_n = 1000$						
$1 - \mathcal{E}$	10^{-5}	10^{-6}	10^{-7}	10^{-8}	10^{-9}	10^{-10}
$\lg(1 - \mathcal{E})$	-5	-6	-7	-8	-9	-10
\mathcal{E}_0 , mV/cm	0.04999995	0.04999995	0.049999995	0.0499999995	0.04999999995	0.049999999995
$\lg v_0$	-5/2	-3	-7/2	-4	-9/2	-5
v_0	$10^{-5/2}$	10^{-3}	$10^{-7/2}$	10^{-4}	$10^{-9/2}$	10^{-5}
v , nm/s	$3.166 \times 10^{7/2} = 10^4$	3.166×10^3	$3.166 \times 10^{3/2} = 10^3$	3.166×10^2	$3.166 \times 10^{3/2} = 10^2$	31.66
$N_n = 40$						
$1 - \mathcal{E}$	10^{-5}	10^{-6}	10^{-7}	10^{-8}	10^{-9}	10^{-10}
$\lg(1 - \mathcal{E})$	-5	-6	-7	-8	-9	-10
\mathcal{E}_0 , V/cm	0.04999995	0.04999995	0.049999995	0.0499999995	0.04999999995	0.049999999995
$\lg v_0$	-5/2	-3	-7/2	-4	-9/2	-5
v_0	$10^{-5/2}$	10^{-3}	$10^{-7/2}$	10^{-4}	$10^{-9/2}$	10^{-5}
v , nm/s	$6.33 \times 10^{3/2} = 2000$	$6.33 \times 10^2 = 633$	$6.33 \times 10^{3/2} = 200$	63.3	20	6.33
$N_n = 10$						
$1 - \mathcal{E}$	10^{-5}	10^{-6}	10^{-7}	10^{-8}	10^{-9}	10^{-10}
$\lg(1 - \mathcal{E})$	-5	-6	-7	-8	-9	-10
\mathcal{E}_0 , V/cm	0.04999995	0.04999995	0.049999995	0.0499999995	0.04999999995	0.049999999995
$\lg v_0$	-5/2	-3	-7/2	-4	-9/2	-5
v_0	$10^{-5/2}$	10^{-3}	$10^{-7/2}$	10^{-4}	$10^{-9/2}$	10^{-5}
v , nm/s	$3.166 \times 10^{3/2} = 10^3$	317	$3.166 \times 10^{3/2} = 100$	32	$3.166 \times 10^{3/2} = 10$	3

low values of \mathcal{E}_0 and for short DNA (low values of N_n). For comparison in **Table 2** is presented some literature data of DNA translocation speed.

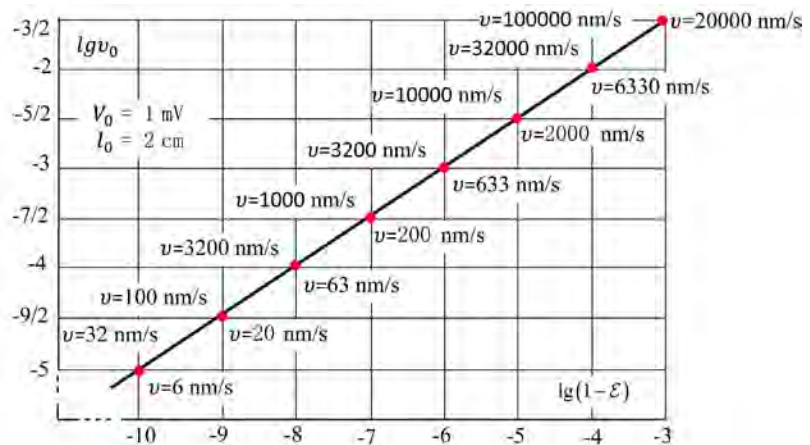
The comparison of the results of **Table 1** and **Table 2** shows the advantage of the proposed method of reducing the translocation speed. Speed control is achieved through the accurate compensation of gravity and drag forces. This can be achieved by controlling the potential of the reference electrode. By adjusting the size of DNA molecule and increasing the accuracy of changing of the reference electrode potential, the translocation speed can be significantly reduced (see cases $N_n = 40$ or 10).

In **Figure 3** the logarithmic dependency of dimensionless DNA translocation speed vs. dimensionless field \mathcal{E} is presented for the case $N_n = 40$ according to data of **Table 1**. This graph built for the case of the optimal values of $V_0 = 0.001$ V and $l_0 = 0.02$ m. In this linear dependency it also shows corresponding values of DNA molecule translocation speed in nm/s units for several values of $\lg(1 - \mathcal{E})$.

The main difficulty of such way to decrease translocation speed conditioned

Table 2. Literature data of DNA translocation speed.

DNA read speed, bases/s (nm/s)	10 - 1000	9600	55,000	70,000,000
References	[7]	[8]	[10]	[33]

**Figure 3.** Logarithmic dependency of DNA translocation dimensionless speed vs. dimensionless electric field. It is shown values of molecules speed in nm/s for the case $N_n = 40$ (the data on the right site) and $N_n = 1000$ (the data on the left site).

by the very slightly changing of electric field \mathcal{E}_0 . The translocation velocity varies also depend on parameters such as the electrical potential, the type of nanopore, and whether the DNA is single-stranded or double-stranded (see also [34]).

Elevator Method

An alternative method for reducing DNA translocation time can be the so-called “elevator method”. By the elevator method, we mean the situation when the nanopore construction (metallic electrodes) moves parallel to Z axis along with the DNA (Figure 1). Moreover, the speed of movement of a nanopore must be approximately equal to or slightly weaker than the speed of movement of DNA. The “elevator method” can be easily implemented in Space (in the Shuttle) without gravity. At the same time, the depth of the cell with an aqueous solution must be quite large so that during the time of passage of the nanopore, at least several DNA molecules can pass through the pore. In this case, the time of passage of the molecule around the electrodes will increase, and the time it takes to read the molecule will be relatively long. The movement of the electrodes can only be adjusted mechanically. Regulation of the pore movement speed by electromagnetic forces is probably impossible, because firstly the electrodes themselves are charged and secondly, they must move in the field created by the potential V_0 .

3. DNA Molecules Reading (Translocation) Time

Time for DNA molecules reading (translocation) can be set by the duration of

the electric pulse on the metal electrodes (see [6]). Denote this time by t_r .

By the sizes of gap between nucleotides $d_0 = 0.34$ nm (see [35]) we can determine the time of absence of the applied impulses on the metallic electrodes [6]. This time can be calculated according to formula $t_g = d_0/\nu$, or

$$t_g = d_0 \left[\frac{m_0 + \rho C_D A l_0}{2(m_0 g l_0 - q V_0)} \right]^{1/2}, \quad (13)$$

The period of the pulses applied to the gold electrodes will be

$$T = t_r + t_g. \quad (14)$$

The frequency of the base's passes (*i.e.* electrical pulses applied to lateral gold electrodes) will be

$$f = \frac{1}{2\pi T} = \frac{1}{2\pi(t_r + t_g)}. \quad (15)$$

Here t_r is the time for DNA molecules bases (A, T, C or G) reading (translocation), and

$$t_r = h_{A(T,C,G)}/\nu, \quad (16)$$

$h_{A(T,C,G)}$ is the vertical size of corresponding nucleotides ($h_{A(T,C,G),\max} = h_C = 0.583$ nm [see Appendix]), $d_0 = 0.34$ nm is the size of gap between nucleotides [35].

Example 1: $V_0 = 0.001$ V and $l_0 = 0.02$ m, $N_n = 40$; $1 - \mathcal{E} = 10^{-6}$, and $\nu = 633$ nm/s, we get $f \approx 110$ Hz, $t_r \approx 9 \times 10^{-4}$ s = 0.9 ms; $1 - \mathcal{E} = 10^{-5}$, and $\nu = 2000$ nm/s, we get $f \approx 345$ Hz, $t_r \approx 3 \times 10^{-4}$ s = 0.3 ms.

Example 2: $V_0 = 0.001$ V and $l_0 = 0.02$ m, $N_n = 1000$; $1 - \mathcal{E} = 10^{-6}$, and $\nu = 3170$ nm/s, we get $f \approx 547$ Hz; $t_r \approx 2 \times 10^{-4}$ s = 0.2 ms; $1 - \mathcal{E} = 10^{-5}$, and $\nu = 10,000$ nm/s, we get $f \approx 1725$ Hz; $t_r \approx 6 \times 10^{-5}$ s = 0.06 ms.

If t is the passing full time for one DNA molecule through nanopore and N_n is the number of bases groups in DNA, we can write

$$\nu = \frac{l_{\text{DNA}}}{t}, \quad (17)$$

where

$$l_{\text{DNA}} = N_n(h_A + h_T + h_G + h_C) + (N_n - 1)d_0 \quad (18)$$

is the DNA total length consisting only groups with four bases. Here $h_A = 0.480$ nm, $h_T = 0.504$ nm, $h_G = 0.514$ nm and $h_C = 0.583$ nm are the sizes in direction of Z axis of adenine, thymine, guanine and cytosine, correspondingly (see Appendix).

In the other hand

$$t = N_n t_r + (N_n - 1)t_g. \quad (19)$$

For example, for the case $t_r = 3 \times 10^{-4}$ s, $t_g = 5.37 \times 10^{-4}$ s and $N_n = 40$, we get $t \approx 0.031$ s.

It is quite large and measurable time for reading of DNA sequencing.

We can control value of t_r and f by the choice magnitudes of V_0 and I_0 . For comparison note that in Ref. [7] the reasonable value of the DNA translocation speed is near to 0.01 - 1 ms per base considered. It is more short time compared with 0.031 s. Note that all of the biological and synthetic nanopores have barrels of ~ 5 nm (which is considerably longer than the base-to-base distance of 3.4 Å) in thickness and accommodate $\sim 10 - 15$ nucleotides at a time. It is, therefore, impossible to achieve single-base resolution using blockage current measurements. In addition, the average rate at which a polymer typically translocates through a nanopore is on the order of 1 nucleotide/ μs (*i.e.*, on the order of MHz detection), which is too fast to resolve.

4. Conclusions

Solid-state nanopore DNA sequencing modified method is developed and presented. The nanogap is made on gold electrodes in the form of nanowires or nanoribbons. A detailed analysis of the dynamics of a DNA molecule in an aqueous solution is carried out. For the first time in analytical calculations, all forces acting on DNA molecules are taken into account. The movement of DNA in aqueous solution is regulated by the potential applied to reference electrode. Taking into consideration that DNA moves under gravity, electrophoretic and drag forces of the expression for the DNA translocation speed are calculated and analyzed. The conditions for decreasing the DNA translocation speed or increasing reading time are received. Carried numerical calculations show that increasing the reading time is associated with the problem of very subtle regulation of the electric field strength acting on DNA molecule.

Based on the modified method proposed above it is possible to successfully decrease molecule translocation time and increase its reading time. It will give possibility of enlarging the passing time of tunnel current through gold-nucleotide-gold junction and more precisely determine and identify nucleotide type crating an electrical bridge between electrodes [6]. Our results therefore potentially suggest a realistic, inherently design-specific, high-throughput nanopore DNA sequencing device/cell as a de-novo alternative to the existing methods.

The amount of tunnel current which can pass through the nanopore at any given moment therefore varies depending on whether the nanopore is bounded by an A, T, C or G nucleotide. The change in the current through the nanopore as the DNA molecule passes through the nanopore represents a direct reading of the DNA sequence. Such behavior is ordinary. Analyses of the tunnel currents responsible for nitrogenous bases in DNA are developed and presented by us in [6].

It has been shown that one can control value of the DNA molecules bases reading time and the frequency of the electrical pulses applied to lateral electrodes by the choice of magnitude of the potential of the reference electrode. It is shown that DNA reading time can be quite large and measurable value in order to 10^3 bases/s. The conditions of lengthening of the reading time are determined.

Author Contribution Information

All authors participated in the statement of the problem and discussion of the results. L. Gasparyan, I. Mazo and F. Gasparyan conducted literature review. F. Gasparyan and V. Simonyan made calculations and participated in the writing of the text of the article.

Conflicts of Interest

The authors declare no conflicts of interest regarding the publication of this paper.

References

- [1] Munshi, A. (2012) DNA Sequencing—Methods and Applications. InTech, London.
- [2] Rincon-Restrepo, M., Mikhailova, E., Bayley, H. and Maglia, G. (2011) Controlled Translocation of Individual DNA Molecules through Protein Nanopores with Engineered Molecular Brakes. *Nano Letters*, **11**, 746-750. <https://doi.org/10.1021/nl1038874>
- [3] Howorka, S., Cheley, S. and Bayley, H. (2001) Sequence-Specific Detection of Individual DNA Strands Using Engineered Nanopores. *Nature Biotechnology*, **19**, 636-639. <https://doi.org/10.1038/90236>
- [4] Zahid, O.K., Wang, F., Ruzicka, J.A., Taylor, E.W. and Hall, A.R. (2016) Sequence-Specific Recognition of microRNAs and Other Short Nucleic Acids with Solid-State Nanopores. *Nano Letters*, **16**, 2033-2039. <https://doi.org/10.1021/acs.nanolett.6b00001>
- [5] Clamer, M., Höfler, L., Mikhailova, E., Viero, G. and Bayley, H. (2014) Detection of 3'-end RNA Uridylation with a Protein Nanopore. *ACS Nano*, **8**, 1364-1374. <https://doi.org/10.1021/nn4050479>
- [6] Gasparyan, L., Mazo, I., Simonyan, V. and Gasparyan, F. (2020) Study of Molecular Junctions Metal-DNA-Metal for DNA Sequencing. *Journal of Contemporary Physics (Armenian Academy of Sciences)*, **55**, 77-86. <https://doi.org/10.3103/S1068337220010119>
- [7] Fologea, D., Uplinger, J., Thomas, B., McNabb, D.S. and Li, J. (2005) Slowing DNA Translocation in a Solid-State Nanopore. *Nano Letters*, **5**, 1734-1737. <https://doi.org/10.1021/nl051063o>
- [8] Peng, H.B. and Ling, X.S.S. (2009) Reverse DNA Translocation through a Solid-State Nanopore by Magnetic Tweezers. *Nanotechnology*, **20**, Article ID: 185101. <https://doi.org/10.1088/0957-4484/20/18/185101>
- [9] McCormick, B.W. (1979) Aerodynamics, Aeronautics, and Flight Mechanics. John Wiley & Sons, Inc., New York. https://en.wikipedia.org/wiki/Drag_coefficient
- [10] He, Y., Tsutsui, M., Fan, C., Taniguchi, M. and Kawai, T. (2011) Controlling DNA Translocation through Gate Modulation of Nanopore Wall Surface Charges. *ACS Nano*, **5**, 5509-5518. <https://doi.org/10.1021/nn201883b>
- [11] Meller, A. (2003) Dynamics of Polynucleotide Transport through Nanometre-Scale Pores. *Journal of Physics: Condensed Matter*, **15**, R581-R607. <https://doi.org/10.1088/0953-8984/15/17/202>
- [12] Meller, A., Nivon, L., Brandin, E., Golovchenko, J. and Branton, D. (2000) Rapid Nanopore Discrimination between Single Oligonucleotide Molecules. *Proceedings*

- of the National Academy of Sciences of the United States of America, **97**, 1079-1084. <https://doi.org/10.1073/pnas.97.3.1079>
- [13] Mathe, J., Aksimentiev, A., Nelson, D.R., Schulten, K. and Meller, A. (2005) Orientation Discrimination of Single-Stranded DNA inside the α -Hemolysin Membrane Channel. *Proceedings of the National Academy of Sciences of the United States of America*, **102**, 12377-12382. <https://doi.org/10.1073/pnas.0502947102>
- [14] Chang, S., Huang, S., He, J., Liang, F., Zhang, P., Li, S., Chen, X., Sankey, O. and Lindsay, S. (2010) Electronic Signatures of All Four DNA Nucleosides in a Tunneling Gap. *Nano Letters*, **10**, 1070-1075. <https://doi.org/10.1021/nl1001185>
- [15] Nakane, J., Wiggin, M. and Marziali, A. (2004) A Nanosensor for Transmembrane Capture and Identification of Single Nucleic Acid Molecules. *Biophysical Journal*, **87**, 615-621. <https://doi.org/10.1529/biophysj.104.040212>
- [16] Tropini, C. and Marziali, A. (2007) Multi-Nanopore Force Spectroscopy for DNA Analysis. *Biophysical Journal*, **92**, 1632-1637. <https://doi.org/10.1529/biophysj.106.094060>
- [17] Wanunu, M., Chakrabarti, B., Mathe, J., Nelson, D.R. and Meller, A. (2008) Orientation-Dependent Interactions of DNA with an α -Hemolysin Channel. *Physical Review E*, **77**, Article ID: 031904. <https://doi.org/10.1103/PhysRevE.77.031904>
- [18] Payne, C.M., Zhao, X., Vlcek, L. and Cummings, P. (2008) Molecular Dynamics Simulation of ss-DNA Translocation between Copper Nanoelectrodes Incorporating Electrode Charge Dynamics. *The Journal of Physical Chemistry B*, **112**, 1712-1717. <https://doi.org/10.1021/jp077483e>
- [19] Branton, D., Deamer, D.W., Marziali, A. and Bayley, H. (2008) The Potential and Challenges of Nanopore Sequencing. *Nature Biotechnology*, **26**, 1146-1153. <https://doi.org/10.1038/nbt.1495>
- [20] Gasparyan, L., Mazo, I., Simonyan, V. and Gasparyan, F. (2019) DNA Sequencing: Current State and Prospects of Development. *Open Journal of Biophysics*, **9**, 169-197. <https://doi.org/10.4236/ojbiphy.2019.93013>
- [21] Gasparyan, L., Mazo, I., Simonyan, V. and Gasparyan, F. (2019) ISFET Based DNA Sensor: Current-Voltage Characteristic and Sensitivity to DNA Molecules. *Open Journal of Biophysics*, **9**, 239-253. <https://doi.org/10.4236/ojbiphy.2019.94017>
- [22] Gasparyan, L., Mazo, I., Simonyan, V. and Gasparyan, F. (2020) Noises and Signal-to-Noise Ratio of Nanosize EIS and ISFET Biosensors. *Open Journal of Biophysics*, **10**, 1-12. <https://doi.org/10.4236/ojbiphy.2020.101001>
- [23] Clarke, J., Wu, H.-C., Jayasinghe, L., Patel, A., Reid, S. and Bayley, H. (2009) Continuous Base Identification for Single-Molecule Nanopore DNA Sequencing. *Nature Nanotechnology*, **4**, 265-270. <https://doi.org/10.1038/nnano.2009.12>
- [24] Butler, T.Z., Gundlach, J.H. and Troll, M. (2007) Ionic Current Blockades from DNA and RNA Molecules in the α -Hemolysin Nanopore. *Biophysical Journal*, **93**, 3229-3240. <https://doi.org/10.1529/biophysj.107.107003>
- [25] Perrin, M.L., Verzijl, C.J., Martin, C.A., Shaikh, A.J., Eelkema, R., van Esch, J.H., van Ruitenbeek, J.M., Thijssen, J.M., van der Zant, H.S. and Dulic, D. (2013) Large Tunable Image-Charge Effects in Single-Molecule Junctions. *Nature Nanotechnology*, **8**, 282-287. <https://doi.org/10.1038/nnano.2013.26>
- [26] Xiang, D., Jeong, H., Lee, T. and Mayer, D. (2013) Mechanically Controllable Break Junctions for Molecular Electronics. *Advanced Materials*, **25**, 4845-4867. <https://doi.org/10.1002/adma.201301589>
- [27] Vladyka, A., Perrin, M.L., Overbeck, J., Ferradas, R.R., Garcia-Suarez, V., Gan-

- tenbein, M., Brunner, J., Mayor, M., Ferrer, J. and Calame, M. (2019) *In-Situ* Formation of One-Dimensional Coordination Polimers in Molecular Junction. *Nature Communications*, **10**, 262. <https://doi.org/10.1038/s41467-018-08025-9>
- [28] Binnig, G., Rohrer, H., Gerber, Ch. and Weibel, E. (1982) Surface Studies by Scanning Tunneling Microscopy. *Physical Review Letters*, **49**, 57-61. <https://doi.org/10.1103/PhysRevLett.49.57>
- [29] Binnig, G., Quate, C.F. and Gerber, C. (1986) Atomic Force Microscope. *Physical Review Letters*, **56**, 930-933. <https://doi.org/10.1103/PhysRevLett.56.930>
- [30] Chassaing, P., Antonia, R.A., Anselmet, F., Joly, L. and Sarkar, S. (2002) Variable Density Fluid Turbulence (Fluid Mechanics and Its Applications). Vol. 69, Springer, Berlin. <https://doi.org/10.1007/978-94-017-0075-7>
- [31] Mandelkern, M., Elias, J.G., Eden, D. and Crothers, D.M. (1981) The Dimensions of DNA in Solution. *Journal of Molecular Biology*, **152**, 153-161. [https://doi.org/10.1016/0022-2836\(81\)90099-1](https://doi.org/10.1016/0022-2836(81)90099-1)
- [32] Meller, A., Nivon, L. and Branton, D. (2001) Voltage-Driven DNA Translocations through a Nanopore. *Physical Review Letters*, **86**, 3435-3438. <https://doi.org/10.1103/PhysRevLett.86.3435>
- [33] Smolyanitsky, A., Yakobson, B.I., Wassenaar, T.A., Paulechka, E. and Kroenlein, K. (2016) A MoS₂-Based Capacitive Displacement Sensor for DNA Sequencing. *ACS Nano*, **10**, 9009-9016. <https://doi.org/10.1021/acs.nano.6b05274>
- [34] Steinbock, L.J. and Radenovic, A. (2015) The Emergence of Nanopores in Next-Generation Sequencing. *Nanotechnology*, **26**, Article ID: 074003. <https://doi.org/10.1088/0957-4484/26/7/074003>
- [35] Watson, J.D. and Crick, F.H. (1953) Molecular Structure of Nucleic Acids; a Structure for Deoxyribose Nucleic Acid. *Nature*, **171**, 737-738. <https://doi.org/10.1038/171737a0>
- [36] Pyykkö, P. and Atsumi, M. (2009) Molecular Double-Bond Covalent Radii for Elements Li-E112. *Chemistry: A European Journal*, **15**, 12770-12779. <https://doi.org/10.1002/chem.200901472>

Appendix

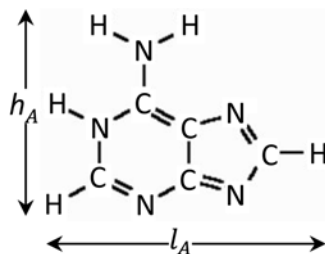
For calculations of nucleosides sizes, we use data for the covalent radii some elements presented in **Table A1** [36].

Table A1. The covalent radii some elements in nm [36].

Element	Single bond	Double bond	Triple bond
H	0.032	-	-
C	0.075	0.067	0.060
N	0.071	0.060	0.054
O	0.063	0.052	0.053

Let's denote the vertical size of the nucleotides through h , and the horizontal size—through l . Indexes H-C (or C-H), C=N etc. means single and double bonds between corresponding elements.

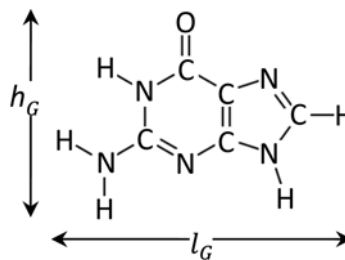
Adenine (C₅H₅N₅)



$$\begin{aligned}
 l_A &= l_{\text{H-C}} \cos 30 + l_{\text{C=N}} \cos 30 + l_{\text{N-C}} \cos 30 + l_{\text{C=N}} \cos 18 + l_{\text{N-C}} \sin 36 + l_{\text{C-H}} \\
 &= [0.107 + 0.127 + 0.146] \times 0.866 + 0.127 \times 0.9511 \\
 &\quad + 0.146 \times 0.5878 + 0.107 \\
 &= 0.3291 + 0.1208 + 0.094 + 0.107 = 0.651 \text{ nm}
 \end{aligned}$$

$$\begin{aligned}
 h_A &= h_{\text{C=N}} \sin 30 + h_{\text{C-N}} + h_{\text{N-C}} \sin 30 + h_{\text{C-N}} + h_{\text{N-H}} \sin 30 \\
 &= (0.067 + 0.06 + 0.075 + 0.071 + 0.032 + 0.071) \times 0.5 \\
 &\quad + 2 \times (0.071 + 0.075) \\
 &= 0.188 + 0.292 = 0.48 \text{ nm}
 \end{aligned}$$

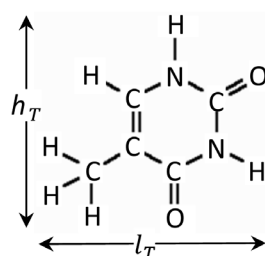
Guanine (CH₅N₅O)



$$\begin{aligned}
 l_G &= h_{\text{H-N}} \cos 30 + h_{\text{N-C}} \cos 30 + h_{\text{C=N}} \cos 30 + h_{\text{N-C}} \cos 30 \\
 &\quad + l_{\text{C-N}} \cos 18 + l_{\text{N-C}} \sin 36 + l_{\text{C-H}} \\
 &= (0.032 + 0.071 + 0.071 + 0.075 + 0.067 + 0.06 + 0.071 + 0.075) \times 0.866 \\
 &\quad + (0.075 + 0.071)(0.9511 + 0.5878) + (0.075 + 0.032) \\
 &= 0.4521 + 0.2247 + 0.082 = 0.784 \text{ nm}
 \end{aligned}$$

$$\begin{aligned}
 h_G &= h_{\text{H-N}} + h_{\text{N-C}} \cos 60 + h_{\text{C=N}} + h_{\text{N-C}} \cos 60 + h_{\text{C=O}} \\
 &= 0.032 + 0.071 + 2 \times 0.5 \times (0.075 + 0.071) \\
 &\quad + 0.075 + 0.071 + 0.067 + 0.052 \\
 &= 0.514 \text{ nm}
 \end{aligned}$$

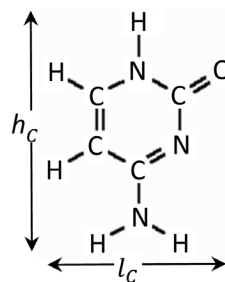
Thymine (C₅H₆N₂O₂)



$$\begin{aligned}
 l_T &= (l_{\text{H-C}} + l_{\text{C-C}} + l_{\text{C-C}} + l_{\text{C-N}} + l_{\text{N-H}}) \times \cos 30 \\
 &= (0.032 + 0.075 + 0.075 + 0.075 + 0.075 + 0.075 \\
 &\quad + 0.075 + 0.071 + 0.071 + 0.032) \times 0.866 \\
 &= 0.656 \text{ nm}
 \end{aligned}$$

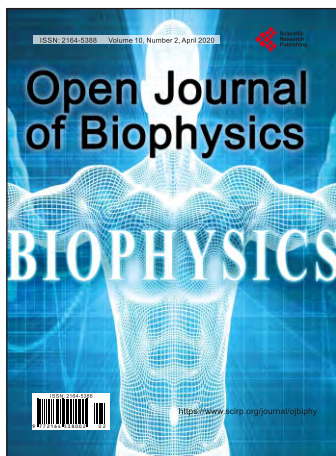
$$\begin{aligned}
 h_T &= h_{\text{O=C}} + h_{\text{C-C}} \sin 30 + h_{\text{C=C}} + h_{\text{C-N}} \sin 30 + h_{\text{N-H}} \\
 &= 0.052 + 0.067 + (0.075 + 0.075 + 0.075 + 0.071) \times 0.5 \\
 &\quad + 0.067 + 0.067 + 0.071 + 0.032 \\
 &= 0.504 \text{ nm}
 \end{aligned}$$

Cytosine (C₄H₅N₃O)



$$\begin{aligned}
 l_C &= l_{\text{H-C}} \cos 30 + l_{\text{C-N}} \cos 30 + l_{\text{N-C}} \cos 30 + l_{\text{C=O}} \cos 30 \\
 &= (0.032 + 0.075 + 0.075 + 0.071 + 0.071 \\
 &\quad + 0.075 + 0.067 + 0.052) \times 0.866 \\
 &= 0.449 \text{ nm}
 \end{aligned}$$

$$\begin{aligned}h_C &= h_{\text{H-N}} \sin 30 + h_{\text{N-C}} + h_{\text{C-C}} \sin 30 + h_{\text{C=C}} + h_{\text{C-N}} \sin 30 + h_{\text{N-H}} \\ &= (0.032 + 0.071 + 0.075 + 0.075 + 0.075 + 0.071) \times 0.5 \\ &\quad + 0.071 + 0.075 + 0.067 + 0.067 + 0.071 + 0.032 \\ &= 0.583 \text{ nm}\end{aligned}$$



Call for Papers

Open Journal of Biophysics

ISSN Print: 2164-5388 ISSN Online: 2164-5396

<https://www.scirp.org/journal/ojbiphy>

Open Journal of Biophysics (OJBIPHY) is an international journal dedicated to the latest advancement of biophysics. The goal of this journal is to provide a platform for scientists and academicians all over the world to promote, share, and discuss various new issues and developments in different areas of biophysics.

Subject Coverage

All manuscripts must be prepared in English, and are subject to a rigorous and fair peer-review process. Accepted papers will immediately appear online followed by printed hard copy. The journal publishes original papers including but not limited to the following fields:

- Bioelectromagnetics
- Bioenergetics
- Bioinformatics and Computational Biophysics
- Biological Imaging
- Biomedical Imaging and Bioengineering
- Biophysics of Disease
- Biophysics of Photosynthesis
- Cardiovascular Biophysics
- Cell Biophysics
- Medical Biophysics
- Membrane Biophysics
- Molecular Biophysics and Structural Biology
- Physical Methods
- Physiology and Biophysics of the Inner Ear
- Proteins and Nucleic Acids Biophysics
- Radiobiology
- Receptors and Ionic Channels Biophysics
- Sensory Biophysics and Neurophysiology
- Systems Biophysics
- Theoretical and Mathematical Biophysics

We are also interested in: 1) Short Reports—2-5 page papers where an author can either present an idea with theoretical background but has not yet completed the research needed for a complete paper or preliminary data; 2) Book Reviews—Comments and critiques.

Notes for Intending Authors

Submitted papers should not have been previously published nor be currently under consideration for publication elsewhere. Paper submission will be handled electronically through the website. All papers are refereed through a peer review process. For more details about the submissions, please access the website.

Website and E-Mail

<https://www.scirp.org/journal/ojbiphy>

E-mail: ojbiphy@scirp.org

What is SCIRP?

Scientific Research Publishing (SCIRP) is one of the largest Open Access journal publishers. It is currently publishing more than 200 open access, online, peer-reviewed journals covering a wide range of academic disciplines. SCIRP serves the worldwide academic communities and contributes to the progress and application of science with its publication.

What is Open Access?

All original research papers published by SCIRP are made freely and permanently accessible online immediately upon publication. To be able to provide open access journals, SCIRP defrays operation costs from authors and subscription charges only for its printed version. Open access publishing allows an immediate, worldwide, barrier-free, open access to the full text of research papers, which is in the best interests of the scientific community.

- High visibility for maximum global exposure with open access publishing model
- Rigorous peer review of research papers
- Prompt faster publication with less cost
- Guaranteed targeted, multidisciplinary audience



Website: <https://www.scirp.org>

Subscription: sub@scirp.org

Advertisement: service@scirp.org